

Analysis and Design of the Output Filter for Buck Envelope Amplifiers

Javier Sebastián*, Pablo Fernández-Miaja*, Alberto Rodríguez* and Miguel Rodríguez**

* Universidad de Oviedo. Grupo de Sistemas Electrónicos de Alimentación (SEA)
Edificio Departamental nº 3. Campus Universitario de Viesques. 33204 Gijón. SPAIN

** Department of Electrical and Computer Engineering
University of Colorado at Boulder. Boulder, Colorado 80309. USA

Abstract: The efficiency of linear power amplifiers can be improved by modulating its supply voltage according to the peak value of the signal that is being amplified in a technique usually known as Envelope Tracking. High bandwidth DC/DC converters called Envelope Amplifiers (EA) are used to carry out the supply modulation in an efficient manner. In the case of linear Radio Frequency Power Amplifiers, the bandwidth requirements over the EA strongly depend on the signal being amplified: in modern telecommunication applications it can range from several hundred kHz to a few tens of MHz. The path to achieve such bandwidths usually goes through increased switching frequencies and/or reduced ratio of switching frequency to converter bandwidth. However, these may lead to lower converter efficiency and increased distortion, making the design of Envelope Amplifiers a challenging task.

This paper addresses the analysis and design of the output filter for Buck converters operating as EA. The output filter must provide enough attenuation at the switching frequency and harmonics to guarantee a desired level of distortion while enabling tracking of wide-bandwidth envelope signals with high converter efficiency. This paper focuses on the use of high-order filters (up to sixth-order Bessel-Thomson, Butterworth and Legendre-Papoulis filters) in a Buck DC/DC converter working as an Envelope Amplifier. The filters are analytically described and characterized, and a design procedure that takes into account the major design constraints is proposed, allowing the selection of the appropriate filter for a given application. The proposed analysis and design method are supported by simulation results, as well as by experiments obtained using a 1 MHz Buck converter operating as an EA.

I. Introduction

The use of Envelope Tracking (ET) techniques has become an attractive option to increase the efficiency of Linear Power Amplifiers (LPAs) [1]-[16]. As it is well known, the maximum theoretical efficiency of a LPA depends on the relationship between the peak value of the signal at its output and its supply voltage. As an example, the maximum theoretical efficiency of a Class-B amplifier based on a pair of complementary bipolar transistors is $\pi/4$ (i.e., 78.5%); this value is reached when the peak output voltage is equal to the

values of the positive-to-ground and the negative-to-ground power supplies. However, if the peak voltage of the signal to be amplified by the LPA varies over time, as it is common in most applications, the average efficiency of the LPA significantly departs from its theoretical maximum. This problem becomes especially severe when the signals to be amplified have a high peak-to-average ratio, as it usually happens in modern digital communication systems that use high data-rate modulations as Quadrature Amplitude Modulation, QAM or standards such as Orthogonal Frequency-Division Multiplexing (OFDM), Enhanced Data rates for GSM Evolution (EDGE), Wideband Code Division Multiple (WCDMA), etc. Thus, efficiencies as low as 10% (and lower) are reported. However, this situation is not only related to the field of Radio Frequency communications, but it is also present in other areas of power electronics [17-18].

The ET technique alleviates this problem by changing the supply voltage of the LPA according to the peak value of the signal being amplified, i.e. by making the supply voltage of the LPA track the envelope of the input signal. Ideally, ET maintains the LPA efficiency as close as possible to its maximum theoretical limit (50% for ideal Class-A LPAs and 78.5% in the case of ideal Class-B LPAs). Figure 1 shows a block diagram of a system that implements ET: the LPA has to be supplied by a DC/DC converter capable of tracking the envelope of the input signal. This converter is usually called Envelope Amplifier (EA). Note that, in the system shown in Fig. 1, the goal is to maximize the overall efficiency. For instance, the efficiency of the LPA can still be increased using the ET technique if the EA is a linear stage; however, the overall system efficiency would typically remain the same, as losses will just move from the LPA to the linear EA. Thus, a switching-mode EA has to be used to improve system efficiency. Many types of switching-mode DC/DC converters have been proposed as EA [1]-[16], but those derived from the basic Buck converter [1], [3], [5], [6], [8]-[16] are especially attractive due to their simplicity, high efficiency and fast dynamic response.

Other techniques that have been proposed to increase the efficiency of Radio Frequency Power Amplifiers (RFPAs), for instance Envelope Elimination and Restoration (EER) [19]-[27], also make use of a DC/DC converter operating as EA, in this case with even more stringent requirements than those needed to implement ET. The general scheme of an amplifier

system using EER is very similar to the one shown in Fig. 1, the main difference being the type of power amplifier used (typically non-linear) and how the signal is split between the EA and the LPA. Thus, the major considerations stated in this work are also applicable to EER.

The transient response of a DC/DC converter strongly depends on its reactive elements. In the case of the Buck converter, these elements are arranged as a low-pass LC filter, which is usually designed to fulfil a certain output voltage ripple specification that depends on the application. It also plays an important role in the dynamic model of the converter, which determines the feedback loop design. DC/DC converters operating as EA must be able to change their output voltage very fast to track wide-bandwidth envelope signals. Assuming that the input voltage of the EA is constant and neglecting the loading effect that the LPA might have over the converter (either because it is considered nearly constant or because it can be compensated for using other techniques), the fastest converter bandwidth can be achieved when it operates in open loop. Once again, Buck converters are especially suitable for this type of operation because they have a linear relationship between the duty cycle and the output voltage (if the input voltage is constant). However, note that this only holds if the converter operates in Continuous Conduction Mode (CCM); the duty cycle to output voltage relationship becomes non-linear when the converter operates in Discontinuous Conduction Mode (DCM) [28]. Therefore, to successfully operate a Buck EA in open loop, CCM operation must be maintained.

This paper addresses the design of the LC output filter for a Buck EA operating in open loop with a constant load. This design is a complex task, as there is a major trade-off between wide-bandwidth tracking capabilities and attenuation of the switching-frequency and its harmonics to avoid signal distortion while maintaining high efficiency operation. High bandwidth could be achieved by increasing the output filter cut-off frequency; however, the switching frequency would have to be further increased to obtain sufficient attenuation of the switching frequency components at the filter output, what in turn leads to lower efficiencies. The end goal of the design

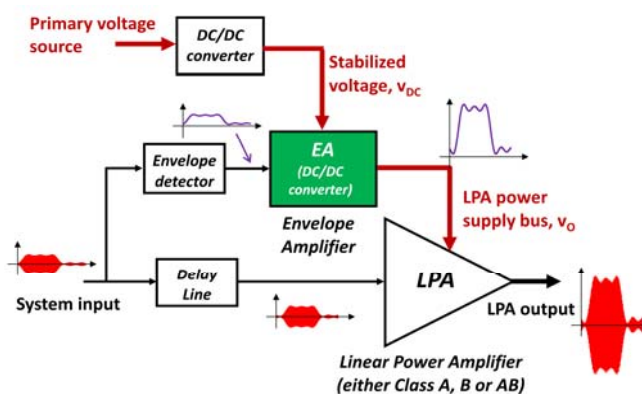


Fig. 1. General scheme for a power amplifier system using the ET technique to improve the overall system efficiency.

process should then be to design a filter that enables the EA to track a certain envelope with as low distortion and as high efficiency as possible. In order to accomplish this, several issues must be addressed:

- Filter type.
- Filter order.
- Ratio between the converter switching frequency and the filter cut-off frequency.
- Either maximum envelope component frequency that can be reproduced with a certain level of distortion, or maximum slew-rate at the EA output.
- Component values for the actual filter implementation.

All these issues will be considered in this paper, which is organized as follows: Section II reviews the classical theory of low-pass filters. The design of low-pass filters for EAs reproducing band-limited envelope signals is studied in Section III, whereas the design of the same filters for the case of broadband envelope signals is presented in Section IV. Section V addresses the implementation of different types (Butterworth, Bessel-Thompson and Legendre-Papoulis) and orders of filters. The conditions to guarantee CCM operation for a certain filter implementation are derived in Section VI, both for steady-state conditions and during transients. A design procedure for the above mentioned filters are presented in Section VII, whereas simulation and experimental results are shown in Section VIII. Finally, Section IX concludes the paper.

II. Review of the classical low-pass filter theory

There are several different types of low-pass filters that have traditionally been defined in terms of their pass-band and stop-band frequency responses (Butterworth, Chebyshev, Bessel-Thomson, Legendre-Papoulis, Cauer, etc.). Chebyshev filters have variable gain in the filter pass-band and Cauer (also called elliptic) filters have a huge rejection of specific frequencies, but they cannot guarantee enough rejection for a wide range of frequencies. Due to this, Chebyshev and Cauer type filters are not suitable to be used as output filter of a Buck DC/DC EA. Three main families of low-pass filters, namely Bessel-Thomson, Butterworth and Legendre-Papoulis, have appropriate pass-band and stop-band frequency characteristics for this application and thus are considered in this paper.

The standard transfer functions of the aforementioned filters can be found in many text books [29]-[31]. The gain of these filters up to order six is plotted in Fig. 2. As this figure shows for any type of filter, the higher the order the higher the slope of the transfer functions in the stop-band, i.e., the higher the attenuation for a given pass-band frequency. Moreover, for a given filter order, Butterworth filters have better stop-band attenuation than Bessel-Thomson, but worse than Legendre-Papoulis. However, Bessel-Thomson filters exhibit superior behaviour regarding the group delay. The group delay $\tau(\omega)$ is defined as:

$$\tau(\omega) = -d\phi(\omega)/d\omega, \quad (1)$$

where $\phi(\omega)$ is the phase of the filter transfer function. A constant group delay in the filter pass-band guarantees that all the frequency components of the signal will experience equal

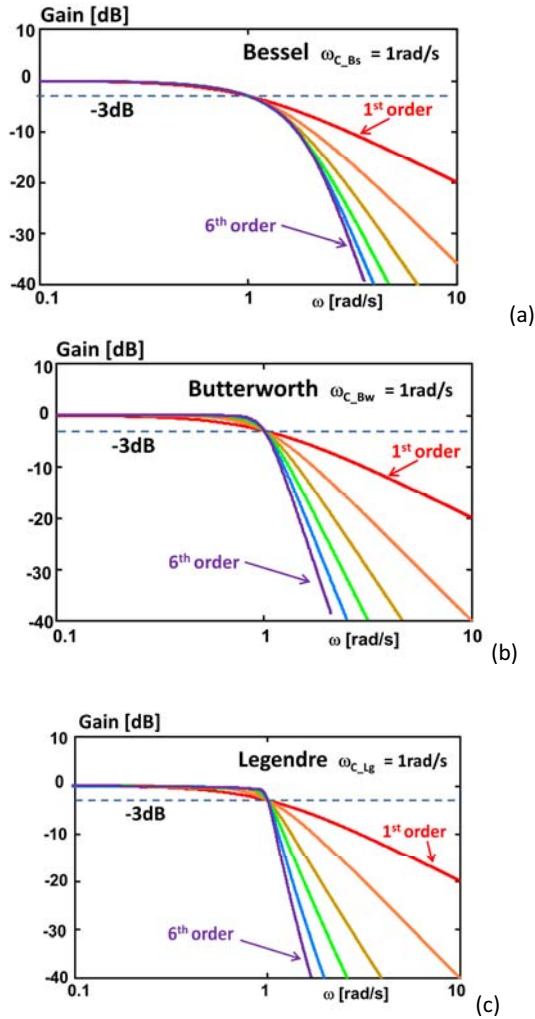


Fig. 2. Gain of the three types of filter under study: a) Bessel-Thomson; b) Butterworth; c) Legendre-Papoulis. In all cases, the angular cut-off frequency is 1 rad/s.

delay. A constant group delay in the pass-band can easily be compensated at a system level and usually leads to lower signal distortion. If the group delay changes considerably in the filter pass-band, the output voltage waveform can experience significant distortion. To quantify the relative variation of the group delay respect to the group delay at DC, the following parameter is defined:

$$\tau_{r0}(\omega) = [\tau(\omega) - \tau(0)]/\tau(0). \quad (2)$$

The values of $\tau_{r0}(\omega)$ for the three filter families are shown in Fig. 3: it can be seen that Bessel-Thomson filters exhibit the best performance.

In summary, Bessel-Thomson filters exhibit the best performances regarding the relative variation of the group delay, but their attenuation in the stop-band is the worst. On the other hand, Legendre-Papoulis filters exhibit just the opposite characteristics, whereas Butterworth filters have performances close to those of the Legendre-Papoulis filters, but less pronounced. Next Section proposes a design procedure that includes group delay and stop-band attenuation

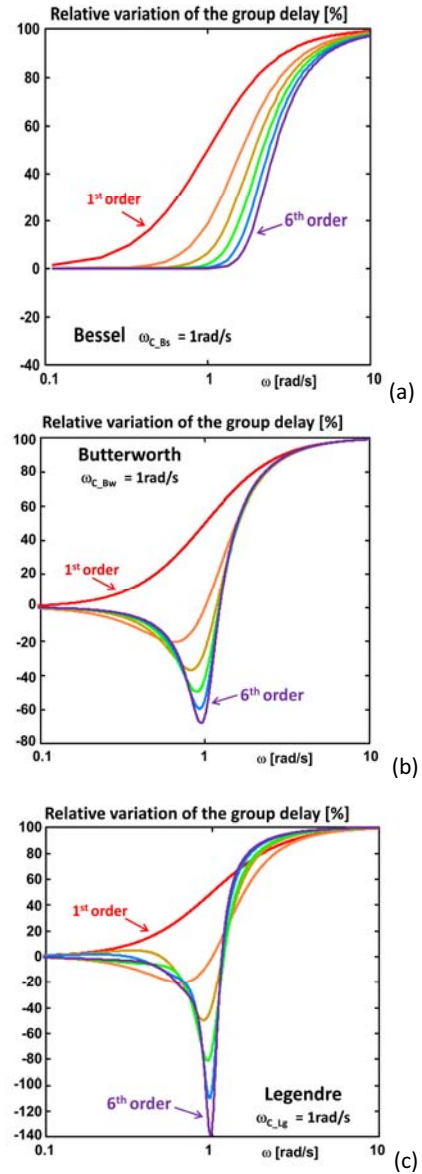


Fig. 3. Relative variation of the group delay, $\tau_{r0}(\omega)$: a) Bessel-Thomson; b) Butterworth; c) Legendre-Papoulis. In all cases, the angular cut-off frequency is 1 rad/s.

characteristics to select the optimum filter family for a given signal bandwidth and allowable distortion.

III. Design of low-pass filters for Envelope Amplifiers reproducing band-limited signals

Figure 4 shows a Buck converter with an n-order output filter. The voltage across the diode v_D is also the input voltage of the filter. As Fig. 5a shows, v_D is a square waveform that is pulse-wide modulated with the information of the envelope signal. The spectrum of v_D is given in Fig. 5b. This spectrum contains the baseband envelope signal, as well as the switching frequency, its harmonics and side-bands [32] and [33]. In this case, the envelope signal has been assumed to be band-limited, ω_{h_max} been the angular frequency of its highest spectral component. The bandwidth of the envelope signal is

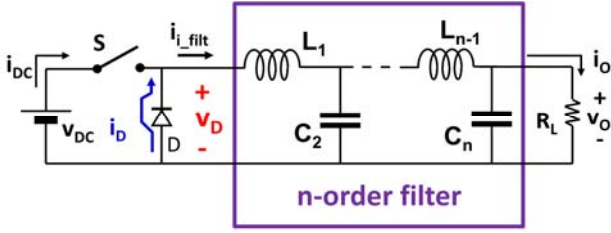


Fig. 4. General scheme of a Buck converter with an n -order low-pass filter at its output.

often limited in practice at a system level due to the real bandwidth limitations of any switching-mode converter when reproducing that envelope signal due to Nyquist-Shannon sampling theorem. In fact, additional linear stages are sometimes connected either in series or in parallel [14] and [15] to the switching-mode EA in order to increase the total bandwidth, in spite of the decrease in efficiency that the use of a linear stage implies.

The spectrum of the envelope signal must be inside the pass-band of the filter, which is defined by its angular cut-off frequency ω_c . Therefore, ω_{h_max} must satisfy:

$$\omega_{h_max} \leq \omega_c. \quad (3)$$

On the other hand, the angular switching frequency ω_s and its harmonics and side-bands must be inside the stop-band of the filter. Neglecting the effects of the components corresponding to the lower side-band near ω_s , ω_s must verify:

$$\omega_c < \omega_s. \quad (4)$$

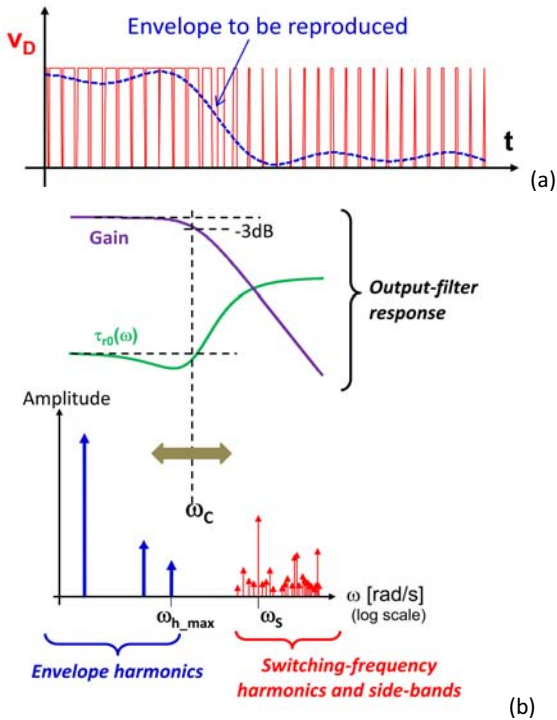


Fig. 5. a) Waveform at the input of the output filter. b) Harmonics corresponding to that waveform.

The design of the filter implies placing ω_c between ω_{h_max} and ω_s in such a way that ω_{h_max} is reproduced with as low distortion as possible, which includes providing sufficient attenuation at the switching frequency and above. Note that both group delay and attenuation at the switching frequency impact signal distortion. However, group delay directly distorts the signal being transmitted, while poor switching frequency attenuation normally causes spectral broadening and out of band noise [34].

Throughout this section, the angular frequency of the maximum spectral component of the envelope signal is normalized to 1 rad/s, i.e., $\omega_{h_max} = 1$ rad/s. A first design attempt is to select $\omega_c = \omega_{h_max} = 1$ rad/s. In this case, the angular frequency ω_{h_max} will be attenuated 3 dB, no matter the filter type and order selected. However, the relative variation of the group delay $\tau_{ro}(\omega)$ is very different for each type of filter, as Fig. 3 shows, and thus its effect on the signal distortion has to be quantified.

To illustrate the influence of $\tau_{ro}(\omega)$ on a real band-limited waveform, a simple example waveform has been used to compare the different filter families. This waveform is a square waveform (duty cycle 0.5) whose harmonic content has been limited to the fifth order harmonic. The angular frequency of the fifth order harmonic ω_{h_max} has been set to 1 rad/s, and thus the angular frequencies of the test waveform are $\omega_1 = 1/5$ rad/s, $\omega_3 = 3/5$ rad/s and $\omega_5 = \omega_{h_max} = 1$ rad/s. The test waveform can be expressed as:

$$v_{env_test}(t) = 1 + \cos[(1/5) \cdot t] - (1/3) \cdot \cos[(3/5) \cdot t] + (1/5) \cdot \cos(t) \quad (5)$$

Figure 6 shows the waveforms at the output of the fourth-order versions of the filters under study when the aforementioned test signal has been introduced at the input. In what follows, the output waveforms of the filters are always delayed an amount corresponding to the group delay introduced by the filter at DC, $\tau(0)$, assuming as mentioned before that this can easily be compensated at a system level. The comparison between the input and output signals clearly shows that the Bessel-Thomson filter has superior performance.

However, this conclusion does not take into account the attenuation provided by the filters at the switching frequency. For instance, in the aforementioned design conditions the Bessel filter provides 40 dB of attenuation at $\omega_{40dB} = 4.723$ rad/s, while Butterworth and Legendre-Papoulis filters provide more than 53 dB and are thus over designed. To establish a fair comparison, the cut-off frequencies of the Butterworth and Legendre-Papoulis filters (ω_{c_Bw} and ω_{c_Lg} , respectively) are increased such that all the filters provide the same 40 dB of attenuation at the angular frequency $\omega_{40dB} = 4.723$ rad/s. To obtain the new filter transfer functions, s must be replaced with s/ω_{c_Bw} (Butterworth) or s/ω_{c_Lg} (Legendre-Papoulis) in the transfer functions given in [29]-[31]. The cut-off frequency of the Bessel-Thomson filter is still $\omega_{c_Bs} = 1$ rad/s, whereas now $\omega_{c_Bw} = 1.494$ rad/s and $\omega_{c_Lg} = 1.821$ rad/s. In these conditions, the response of the modified fourth-order filters to v_{env_test} is shown in Fig. 7; it can be seen that Butterworth and

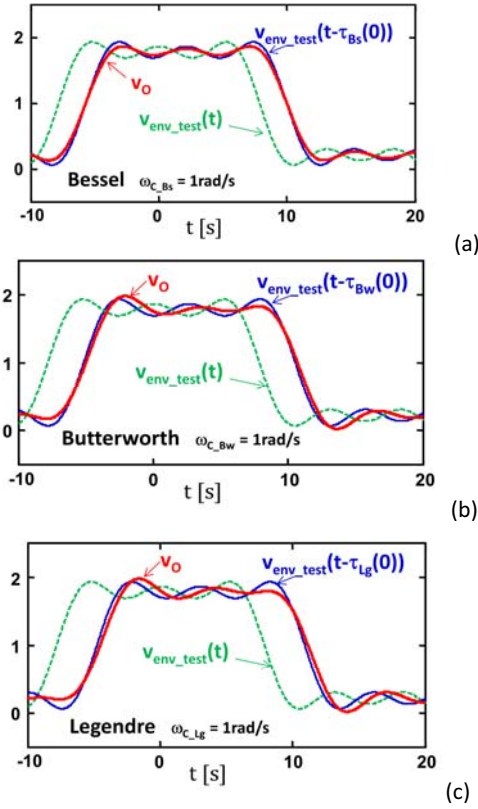


Fig. 6. Response of the fourth-order versions of the filters under study when a test envelope waveform is introduced at their outputs. a) Bessel-Thomson. b) Butterworth. c) Legendre-Papoulis. The values of the group delays at $\omega = 0$ are $\tau_{Bs}(0) = 2.114$ s, $\tau_{Bw}(0) = 2.613$ s and $\tau_{Lg}(0) = 3.041$ s. In all cases, the angular cut-off frequency is 1 rad/s.

Legendre-Papoulis filters (Fig. 7) exhibit superior performance compared to Bessel-Thomson (Fig. 6c).

To further clarify the behaviour presented by the filters in the former design condition (i.e. $\omega_{c_{Bs}} = \omega_{c_{Bw}} = \omega_{c_{Lg}} = 1$ rad/s) and in the latter ($\omega_{c_{Bs}} = 1$ rad/s, $\omega_{c_{Bw}} = 1.494$ rad/s and $\omega_{c_{Lg}} = 1.821$ rad/s), Fig. 8 shows the highest spectral component of the input signal at the filter output, $v_{o_{5th}}(t)$, and the same component at the filter input, $v_{i_{5th}}(t)$. As Figure 8 shows, when the filters are designed to provide the same attenuation at $\omega_{40dB} = 4.723$ rad/s, Butterworth or Legendre-Papoulis filters clearly overcome Bessel-Thomson filters in terms of signal distortion. Note that the angular frequency $\omega_{40dB} = 4.723$ rad/s would typically correspond to the angular switching frequency of the EA.

Furthermore, from the results in Figs. 8a, 8d and 8e, it can be concluded that the waveform corresponding to the Bessel-Thomson filter exhibits almost no delay, but significant attenuation (3 dB, because $\omega_{c_{Bs}} = \omega_{h_{max}} = 1$ rad/s). On the other hand, output waveforms from Butterworth and Legendre-Papoulis filters are slightly delayed, but show negligible attenuation due to their higher cut-off frequency. Therefore, the attenuation has more impact on the error between the input and output waveforms than the variation of the group delay. It should be noted that, as it has been

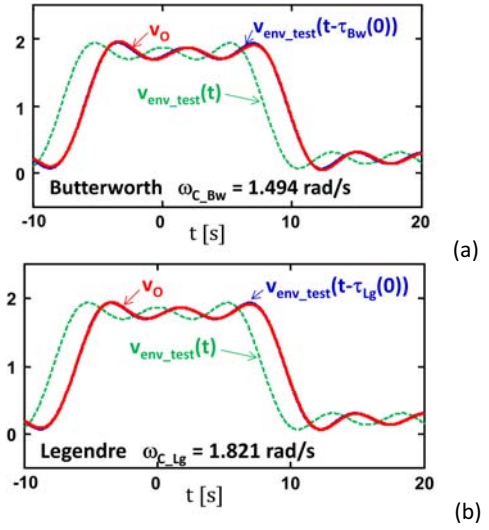


Fig. 7. Response of the fourth versions of the Butterworth filter (a) and Legendre-Papoulis filter (b) when the angular cut-off frequencies are 1.494 rad/s and 1.821 rad/s, respectively. The group delays at $\omega = 0$ are $\tau_{Bw}(0) = 1.749$ s and $\tau_{Lg}(0) = 1.67$ s.

mentioned before, the group delay at a specific frequency (normally at $\omega = 0$) can be compensated in the whole system by delaying the signal at the input of the LPA (see Fig. 1).

The error introduced by the filter can be quantified in a general manner by considering only the highest spectral component of interest of the input signal. When this component is normalized to an angular frequency of $\omega_{h_{max}} = 1$ rad/s, the following quadratic error can be defined:

$$e(\omega_c) = \frac{\frac{1}{2\pi} \int_0^{2\pi} [v_{dis_hmax}(t) - v_{out_hmax}(t, \omega_c)]^2 \cdot dt}{\frac{1}{2\pi} \int_0^{2\pi} [\cos(t)]^2 \cdot dt} = \frac{1}{\pi} \int_0^{2\pi} [v_{dis_hmax}(t) - v_{out_hmax}(t, \omega_c)]^2 \cdot dt, \quad (6)$$

$v_{dis_hmax}(t)$ being the delayed highest spectral component of the input signal:

$$v_{dis_hmax}(t) = \cos[t - \tau(0)], \quad (7)$$

(the amplitude is assumed to be normalized to 1 V) and $v_{out_hmax}(t, \omega_c)$ is the filter output, which is explicitly written as a function of the filter angular cut-off frequency ω_c . Its value is given by:

$$v_{out_hmax}(t, \omega_c) = |H(\omega_c, 1)| \cdot \cos[t + \phi(\omega_c, 1)], \quad (8)$$

where $|H(\omega_c, 1)|$ and $\phi(\omega_c, 1)$ are the filter gain and the filter phase at $\omega_{h_{max}} = 1$ rad/s. Once again the dependence with ω_c is explicitly noted. The values of the error $e(\omega_c)$ for the different design conditions shown in Fig. 8 are 8.6 % for the Bessel-Thomson case, 27.9 % for the Butterworth with $\omega_{c_{Bw}} = 1$ rad/s and 41 % for the Legendre-Papoulis with $\omega_{c_{Lg}} = 1$ rad/s, but this error is as low as only 2.2 % for the Butterworth with $\omega_{c_{Bw}} = 1.494$ rad/s and 0.63 % for the Legendre-Papoulis with $\omega_{c_{Lg}} = 1.821$ rad/s, thus confirming the conclusions qualitatively arising from Fig. 8.

The systematic calculation of this error for the different filter families, up to order six and different values of ω_c leads to the plots shown in Fig. 9. As $\omega_{h_{max}} = 1$ rad/s in all cases, ω_c is

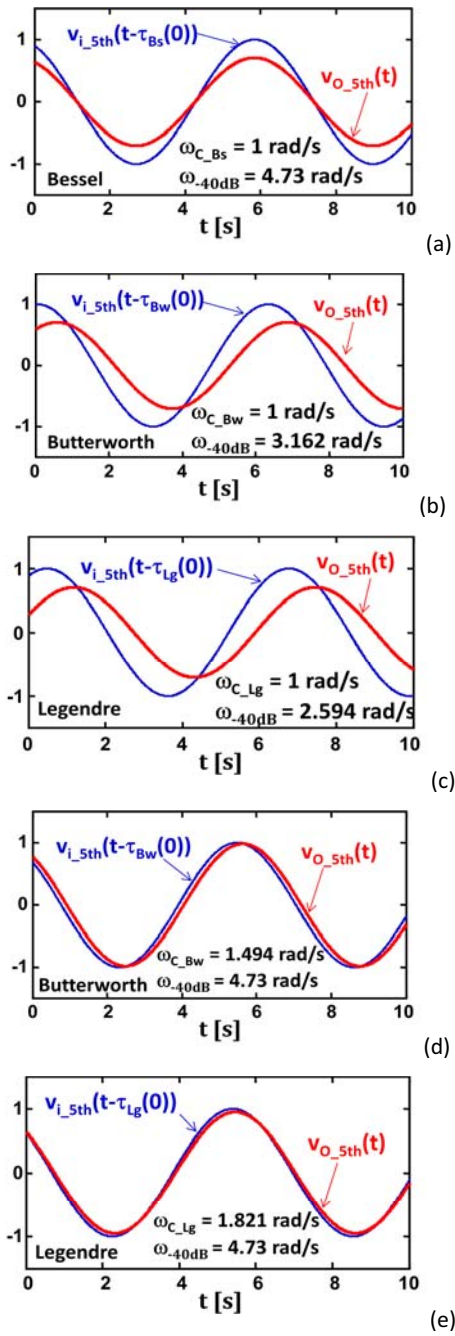


Fig. 8. Reproduction of the fifth harmonic in the example presented in Fig. 6 and Fig. 7. Bessel-Thomson (a), Butterworth (b) and Legendre-Papoulis (c) filters when their cut-off frequencies are 1 rad/s for the three filters. The angular cut-off frequencies has been increased up to 1.494 rad/s in the case of the Butterworth filter (d) and up to 1.821 rad/s in the case of the Legendre-Papoulis filter (e) to have the same attenuation (40 dB) as the Bessel-Thomson filter at 4.723 rad/s.

also the quotient between ω_C and ω_{h_max} , as it appears in these plots. Moreover, the desired attenuation for the angular switching frequency ω_s determines the relationships between

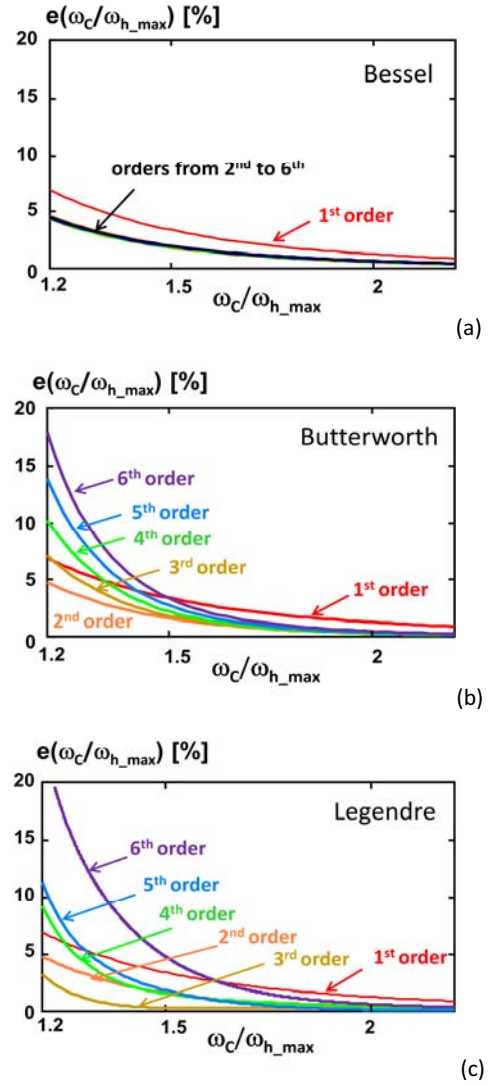


Fig. 9. Quadratic error reproducing the highest order harmonic of a band-limited signal in Bessel-Thomson filters (a), Butterworth filters (b) and Legendre-Papoulis filters (c) as a function of the quotient ω_C/ω_{h_max} .

ω_C and ω_s . These relationships have also been plotted in Fig. 10.

The plots given in Fig. 9 and Fig. 10 allow the selection of the angular cut-off frequency for a given allowed error in the highest spectral component of interest. The design procedure is as follows:

1. Select the type of filter, order and ratio ω_C/ω_{h_max} based on a desired error in the highest spectral component of interest to be reproduced using Fig. 9.
2. Select of the ratio ω_s/ω_C from Fig. 10.
3. Find the ratio ω_s/ω_{h_max} from the previous two values.

It should be noted that the lower this quotient, the higher the efficiency will be, because the switching losses will be lower. However, this quotient has a minimum value imposed by the Nyquist criterion applied to the EA, i.e., this quotient should be higher than 2.

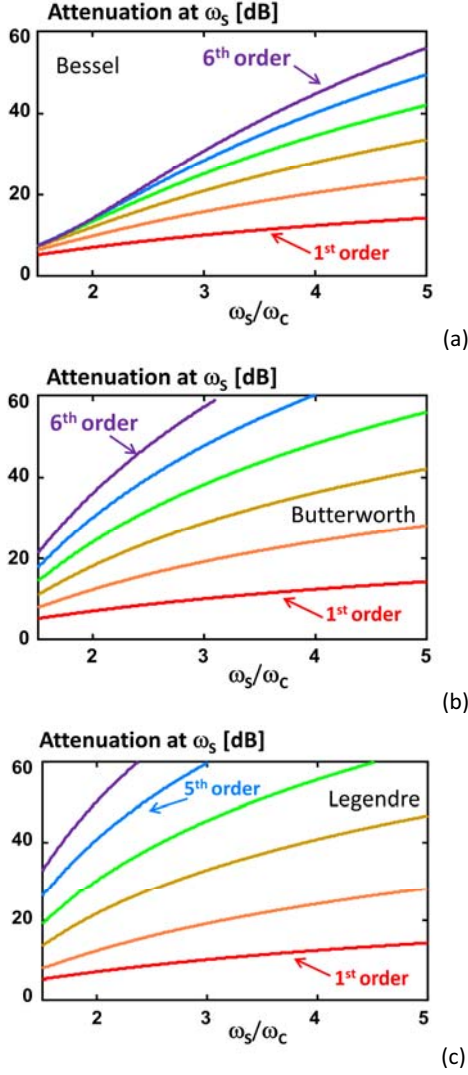


Fig. 10. Attenuation of the angular switching frequency ω_s as a function of the quotient ω_s/ω_c for Bessel-Thomson filters (a), Butterworth filters (b) and Legendre-Papoulis filters (c).

The same information given in the plots shown in Fig. 9 and Fig. 10 is summarized in Fig. 11, where the quotient ω_s/ω_{h_max} directly appears as a function of the desired error for a given attenuation of the angular switching frequency (30 and 40 dB). The value of the quotient ω_s/ω_{h_max} allows us to determine either the EA angular switching frequency ω_s needed to reproduce an envelope signal with a given value of the error $e(\omega_c)$ of its highest-harmonic ω_{h_max} , or the angular frequency ω_{h_max} of the highest harmonic that can be reproduced with a given error $e(\omega_c)$ by an EA working at a given angular switching frequency ω_s . Figure 11 shows that Legendre-Papoulis filters give the best results, followed by Butterworth filters and with Bessel-Thompson in the last place. Furthermore, the plots in Fig. 11 clearly indicate that the use of higher order filters leads to lower ω_s/ω_{h_max} ratio and thus higher EA performance. However, practical considerations impose a limit on the filter order.

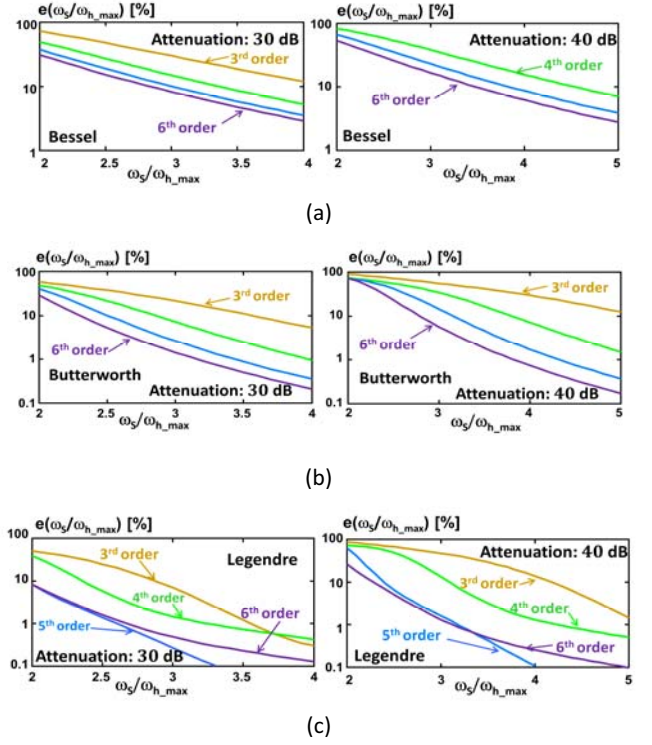


Fig. 11. Quadratic error reproducing the highest-order harmonic of a band-limited signal in Bessel-Thomson filters (a), Butterworth filters (b) and Legendre-Papoulis filters (c) as a function of the quotient ω_s/ω_{h_max} for 30 and 40 dB of switching-frequency attenuation.

IV. An approach to the design of low-pass filters for Envelope Amplifiers reproducing high-slew-rate signals (broadband signals).

If the waveform to be reproduced by the EA cannot be assumed to have a limited bandwidth, the study carried out in the previous section is no longer valid: only harmonic components below $\omega_s/2$ can be reproduced and all the remaining frequency components above that value will experience significant errors. Therefore, it is meaningless to set a given allowed error at a certain frequency. To overcome this conceptual difficulty, a time-domain based approach is used. A time-domain analysis reveals the impact of all the harmonics that cannot be reproduced by the EA.

To test the behaviour of the filters under study in the time domain, a unit step is used as input signal. Figure 12 shows the normalized step responses for the Bessel-Thomson, Butterworth, and Legendre-Papoulis filters when all of them have been designed for the same angular cut-off frequency ω_c . The main variables of interest corresponding to these waveforms are given in Table 1 (Bessel-Thomson), Table 2 (Butterworth) and Table 3 (Legendre-Papoulis). In these tables, $nslw_{0.5}$ is the normalized slew rate, defined as follows:

$$nslw_{0.5} = \left. \frac{d[stp(\omega_c t)]}{d(\omega_c t)} \right|_{t=0.5}, \quad (9)$$

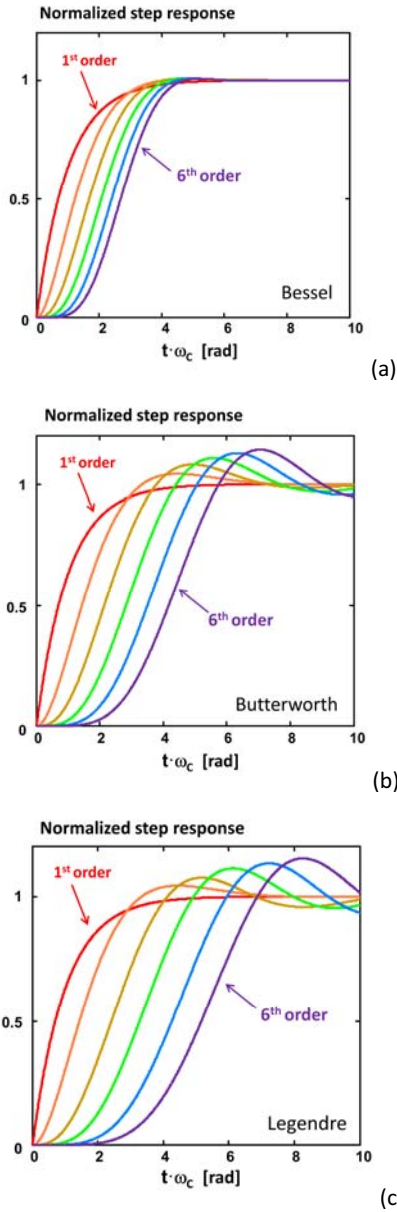


Fig. 12. Normalized step response versus the normalized time $t \cdot \omega_c$ for different types and orders of output filter, all of them designed for the same angular cut-off frequency ω_c : a) Bessel-Thomson filters. b) Butterworth filters. c) Legendre-Papoulis filters.

$stp(\omega_c \cdot t)$ being the normalized step response. The parameter γ is the relative overshoot, whereas $\omega_c \cdot t_{nslw_{0.5}}$ is the normalized time corresponding to $stp(\omega_c \cdot t)$ reaching 50 % of its final value and $\omega_c \cdot t_\gamma$ is the normalized time corresponding to the maximum overshoot.

The actual slew rate just at $t_{nslw_{0.5}}$ when a voltage step V_{step} is applied at the filter input can be easily calculated from $nslw_{0.5}$ as follows:

$$slw_{0.5} = nslw_{0.5} \cdot \omega_c \cdot V_{step} \quad (10)$$

Order	$nslw_{0.5}$	$\omega_c \cdot t_{nslw_{0.5}}$	γ	$\omega_c \cdot t_\gamma$
1 st	0.5 rad ⁻¹	0.693 rad	-	-
2 nd	0.464 rad ⁻¹	1.225 rad	0.433%	4.94 rad
3 rd	0.449 rad ⁻¹	1.681 rad	0.754%	4.714 rad
4 rd	0.444 rad ⁻¹	2.069 rad	0.835%	4.829 rad
5 rd	0.444 rad ⁻¹	2.4 rad	0.773%	5.005 rad
6 nd	0.447 rad ⁻¹	2.686 rad	0.642%	5.194 rad

Table 1. Main normalized variable of the step response of Bessel-Thomson filters.

Order	$nslw_{0.5}$	$\omega_c \cdot t_{nslw_{0.5}}$	γ	$\omega_c \cdot t_\gamma$
1 st	0.5 rad ⁻¹	0.693 rad	-	-
2 nd	0.436 rad ⁻¹	1.433 rad	4.443%	4.321 rad
3 rd	0.404 rad ⁻¹	2.135 rad	8.147%	4.922 rad
4 rd	0.381 rad ⁻¹	2.82 rad	10.833%	5.598 rad
5 rd	0.363 rad ⁻¹	3.496 rad	12.776%	6.313 rad
6 nd	0.349 rad ⁻¹	4.166 rad	14.251%	7.037 rad

Table 2. Main normalized variable of the step response of Butterworth filters.

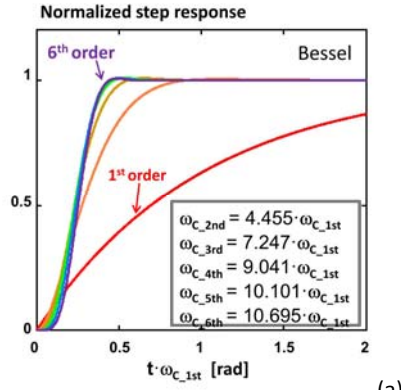
Order	$nslw_{0.5}$	$\omega_c \cdot t_{nslw_{0.5}}$	γ	$\omega_c \cdot t_\gamma$
1 st	0.5 rad ⁻¹	0.693 rad	-	-
2 nd	0.436 rad ⁻¹	1.433 rad	4.443%	4.321 rad
3 rd	0.377 rad ⁻¹	2.41 rad	7.5%	5.161 rad
4 rd	0.352 rad ⁻¹	3.27 rad	11.243%	6.123 rad
5 rd	0.326 rad ⁻¹	4.254 rad	13.275%	7.223 rad
6 nd	0.31 rad ⁻¹	5.158 rad	15.227%	8.25 rad

Table 3. Main normalized variable of the step response of Legendre-Papoulis filters.

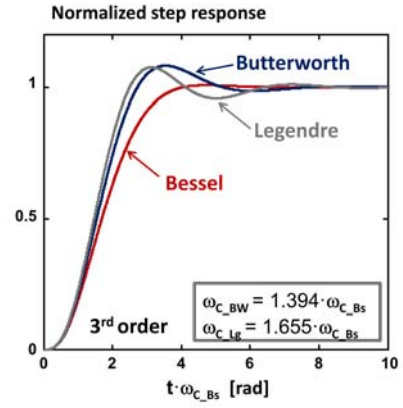
Equation (10) and the values shown in Table 1, Table 2 and Table 3 allow calculating the required value of ω_c for a desired slew rate corresponding to a voltage step of V_{step} volts. Once ω_c is known, ω_s can be found from the plots shown in Fig. 10 for a desired attenuation value. The design procedure can be summarized as follows:

1. Chose filter type, order and ω_c based on the desired slew rate.
2. Chose ω_s based on the desired attenuation at the switching frequency.

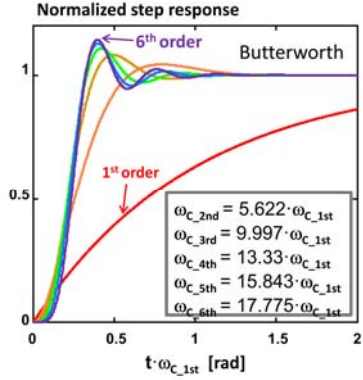
The waveforms in Fig. 12 could easily lead to conclude that low order filters have superior performances compared to high order filters. However, note that results in Fig. 12 have been obtained again neglecting stop-band attenuation. In fact, the step responses shown correspond to very different values of attenuation for a given EA switching frequency. Once again, the design of all the filters can be modified to have the same attenuation, to establish a fairer comparison. As an example, this attenuation has been selected to be 30 dB for the filters



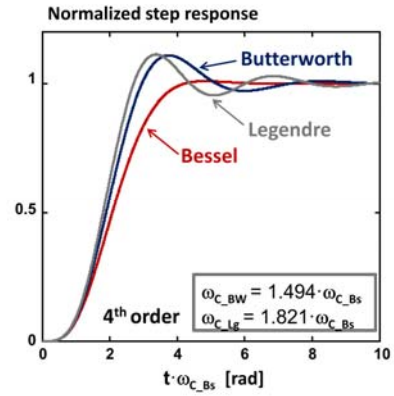
(a)



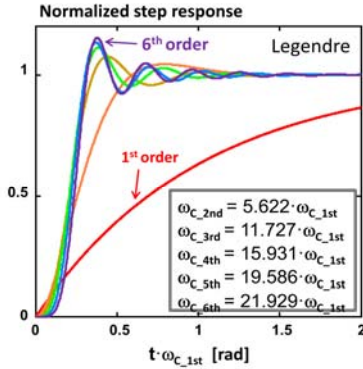
(a)



(b)



(b)



(c)

Fig. 13. Normalized step response of the Bessel-Thomson filters (a), Butterworth filters (b) and Legendre-Papoulis filters (c), versus the normalized time $t \cdot \omega_{C_1st}$, where ω_{C_1st} is the angular cut-off frequency of the first order versions of these filters (which are the same in the three cases). The other angular cut-off frequencies have been selected to have 30 dB of attenuation at the same frequency ($31.607 \cdot \omega_{C_1st}$ rad/s).

whose normalized step response is given in Fig. 13. The value of the angular frequency corresponding to this attenuation, ω_{30dB} , has been chosen using the first order filters as a reference: assuming that the cut-off frequency of a first order filter is ω_{C_1st} rad/s, then $\omega_{30dB} = 31.607 \cdot \omega_{C_1st}$, according to the transfer functions given in [29]-[31]. This definition results advantageous because the three types of filters under study have the same first-order transfer function. Figure 13 shows

Fig. 14. Normalized step response of the third-order (a) and of the fourth-order (b) versions of the filters under study. The angular cut-off frequencies of these filters have been selected to have 40 dB of attenuation at the same frequency, ω_{40dB} . The angular cut-off frequency of the Bessel-Thomson filters ω_{C_Bs} has been used as reference, in such a way that $\omega_{40dB} = 6.47 \cdot \omega_{C_Bs}$ rad/s in the case of the third-order filters and $\omega_{40dB} = 4.723 \cdot \omega_{C_Bs}$ rad/s in the case of the fourth-order filter.

the results with the modified design parameters, where the best performances of the higher order filter can be easily observed, as expected.

The comparison among the different types of filter for a given order is shown in Fig. 14. In this case, the angular cut-off frequency of the Bessel-Thomson filter ω_{C_Bs} is used as reference, whereas the angular cut-off frequency of the Butterworth and Legendre-Papoulis filters (ω_{C_BW} and ω_{C_Lg} , respectively) have been modified (increased) in such a way that all the filters have an attenuation of 40 dB at the same frequency, which is $\omega_{40dB} = 6.47 \cdot \omega_{C_Bs}$ rad/s in the case of the third-order filters and $\omega_{40dB} = 4.723 \cdot \omega_{C_Bs}$ rad/s in the case of the fourth-order filters.

Figures 13 and 14 show that, although Bessel-Thomson filters provide slightly lower slew rate values compared to Butterworth and Legendre-Papoulis, they have almost no overshoot, making them the best choice to be used in the case of EAs. It should be noted that significant overshoot in the output signal may severely increase waveform distortion,

cause spectral broadening and even lead to malfunction of the LPA.

The analysis carried out in Sections III and IV yields two important conclusions. First, Butterworth and Legendre-Papoulis filters are advisable if a band-limited envelope signal is to be reproduced by the EA. A design procedure has been established in this case for any filter selection, where the plots shown in Fig. 9, Fig. 10 and Fig. 11 allow determining ω_C for a given relative error of the highest-order harmonic and, afterwards, the value of the EA angular switching frequency ω_S for a desired attenuation of this frequency. The second conclusion is that the Bessel-Thomson filters exhibit better performance for signals with high slew rate (broadband signals) due to the absence of overshoot when the envelope waveform to be reproduced by the EA experiences very fast variations. Design guidelines have also been provided, where ω_C can be calculated from a desired slew rate (corresponding to an ideal voltage step to be reproduced by the EA) by using (10) and the information shown in Table 1 (for Bessel-Thomson filters). Once ω_C is known, ω_S can be once again obtained from the plots shown in Fig. 10.

V. Implementation of the low-pass filters for Envelope Amplifiers

The theoretical studies carried out in the previous sections of this paper (stop-band attenuation, quadratic errors reproducing a given waveform, step response, etc.) are based on the very well known transfer functions of the three types of low-pass filters under consideration [29]-[31] and they are independent from the physical implementation of these filters, that has not been taken into account yet. In fact, the conclusions obtained so far could be applied to other fields different from the power electronics and the physical implementation of these filters could be based on elements different from inductor and capacitors (for example, operational amplifiers, capacitors and resistors in the case of analog active filters for low frequency applications or transmission lines in the case of filters in the context of the microwave technology).

The implementation of Bessel-Thomson, Butterworth and Legendre-Papoulis low-pass filters based on inductors and capacitors can be easily found in many basic text books [29]-[31]. However, special attention must be paid to the type of voltage source connected at the filter input. In many occasions, the implementations provided by those text books correspond to the case of having an input voltage source v_g with the same value of its output resistance R_g as the one of the load resistance R_L (typically normalized to 1 ohm), as Fig. 15a shows for a fourth order Butterworth filter. The values of the inductors and capacitors required with other values of both resistances R_g and R_L can be easily obtained by simple transformations. However, the aforementioned implementations are not valid in the case of having an ideal voltage source at the filter input, i.e., $R_g = 0 \Omega$. This is because the standard filter implementations in analog signal processing circuits correspond to design the filter matched for maximum power transfer in the pass-band from the real voltage source (made up of v_g and R_g) to the load. The filter implementation based on this criterion is meaningless in the case of an ideal

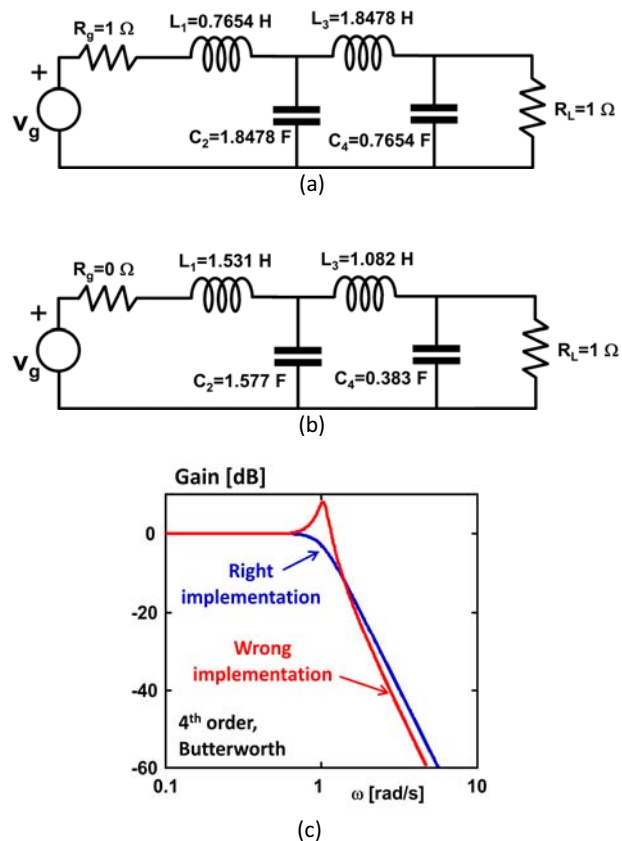


Fig. 15. Right implementations of the fourth-order Butterworth filter with $\omega_C = 1 \text{ rad/s}$ when $R_g = 1 \Omega$ (a) and when $R_g = 0 \Omega$ (b). In both cases, the gain of the filter is the one labeled as “right” in Fig. 15c. However, the gain of the filter becomes incorrect if the implementation corresponding to $R_g = 1 \Omega$ (Fig. 15a) is used with $R_g = 0 \Omega$, as Fig. 15.c shows.

voltage source at the input filter, because the available power of an ideal voltage source is infinity. As a consequence, the filter implementation cannot be based on matching the voltage source and the load for maximum power transfer.

The implementation of low-pass filters having an ideal source at the input port is not new. Thus, the right implementation of these filters when an ideal current source is connected at the input port can be found in [31] and [35]. The interest for this case comes from the years when vacuum tubes were used as active devices in electronics and the filter can be synthesized without any problem in this situation, where the input source and the load are not matched for maximum power transfer. The right values of the filter elements in the case of an ideal voltage source at the input port can be found in some handbooks and text books [31], [35] and [36]. Figure 15b shows the right values of the filter elements for the case of a fourth order Butterworth filter for a source with zero output impedance $R_g = 0 \Omega$. This is the implementation that must be used in the case of the output filter of any Buck DC/DC converter, because the switching network placed at the filter input operates as a nearly ideal square-waveform voltage source when the converter is working in the CCM, and thus

has negligible output impedance compared to R_L (see Fig. 4 and 5).

The implementation of a filter calculated for the case of having $R_g = 1 \Omega$ when the input voltage source has zero output impedance (i.e., $R_g = 0 \Omega$) leads to a significant malfunction of the filter. Fig. 15c shows the gain of a fourth-order Butterworth filter designed for the case of being $R_g = 1 \Omega$ when it is used in a filter with $R_g = 0 \Omega$. As this figure shows, the behaviour is far from the expected from an ideal fourth order Butterworth filter.

Table 4, Table 5 and Table 6 show the normalized values ($R_L = 1$, $\omega_C = 1$) of the inductor (l_x) and capacitor (c_x) for several filter orders and the three filter families under consideration. From these parameters, the actual values of the filter elements for a different angular cut-off frequency ω_C and a load resistance R_L can be easily calculated by denormalizing as follows:

Order	l_1	c_2	l_3	c_4	l_5	c_6
1 st	1	-	-	-	-	-
2 nd	1.36165	0.45384	-	-	-	-
3 rd	1.463	0.84272	0.292671	-	-	-
4 th	1.50109	0.97811	0.61282	0.21139	-	-
5 th	1.51252	1.02315	0.75323	0.47286	0.16191	-
6 th	1.51255	1.03297	0.81237	0.60718	0.37848	0.12868

Table 4. Elements of Bessel-Thomson filters designed with $\omega_C = 1$ rad/s and $R_L = 1 \Omega$.

Order	l_1	c_2	l_3	c_4	l_5	c_6
1 st	1	-	-	-	-	-
2 nd	1.4142	0.7071	-	-	-	-
3 rd	1.5	1.3333	0.5	-	-	-
4 th	1.5307	1.5772	1.0824	0.3827	-	-
5 th	1.5451	1.6944	1.3820	0.8944	0.3090	-
6 th	1.5529	1.7593	1.5529	1.2016	0.7579	0.2588

Table 5. Elements of Butterworth filters designed with $\omega_C = 1$ rad/s and $R_L = 1 \Omega$.

Order	l_1	c_2	l_3	c_4	l_5	c_6
1 st	1	-	-	-	-	-
2 nd	1.4142	0.7071	-	-	-	-
3 rd	1.5909	1.4270	0.7629	-	-	-
4 th	1.6120	1.6616	1.4292	0.6399	-	-
5 th	1.6372	1.7509	1.7358	1.3945	0.6445	-
6 th	1.6348	1.8088	1.8223	1.6795	1.3486	0.5793

Table 6. Elements of Legendre-Papoulis filters designed with $\omega_C = 1$ rad/s and $R_L = 1 \Omega$.

$$L_x = \frac{l_x \cdot R_L}{\omega_C} , \quad (11)$$

$$C_x = \frac{c_x}{\omega_C \cdot R_L} . \quad (12)$$

The values of the elements given in Table 5 and in Table 6 for Butterworth and Legendre-Papoulis low-pass filters have been obtained directly from [31]. However, it is worth noting that the values of l_x and c_x that can be found in [31] for the case of Bessel-Thomson filters are normalized using a group delay of 1 second instead of $\omega_C = 1$. Table 4 shows the values appropriately modified to the normalization $R_L = 1$, $\omega_C = 1$ mentioned above. For example, the values of both the inductors and capacitors given in [31] must be multiplied by 2.11392 in the case of the fourth-order filter.

VI. The conduction mode with high-order low-pass filters

The basic PWM DC/DC converters can operate in the CCM (see Fig. 16a), in the DCM (see Fig. 16b), or in the boundary between these modes, usually called Boundary Conduction Mode (BCM). If the converter has a synchronous rectifier, then only CCM operation can occur (see Fig. 16c). For a Buck converter operating in the CCM, the voltage waveforms at the filter input are as shown in Fig. 5, Fig. 16a and Fig. 16c, i.e., simple square-voltage waveforms whose average value determines the output voltage in steady state. In this case, the output voltage v_O in steady state is a well-known linear function of the duty cycle d_c :

$$v_O = d_c \cdot v_{DC} \quad (13)$$

On the other hand, when the converter is operating in the DCM, the relationship between the output voltage v_O and the duty cycle d_c becomes more complex [28]:

$$v_O = \frac{2 \cdot v_{DC}}{1 + \sqrt{1 + \frac{4 \cdot k}{d_c^2}}} , \quad (14)$$

where k is the conduction mode dimensionless parameter defined in [28]:

$$k = \frac{2L}{R_L \cdot T_s} . \quad (15)$$

As (14) shows, the output voltage v_O in the DCM is no longer a linear function of the duty cycle d_c ; furthermore, in

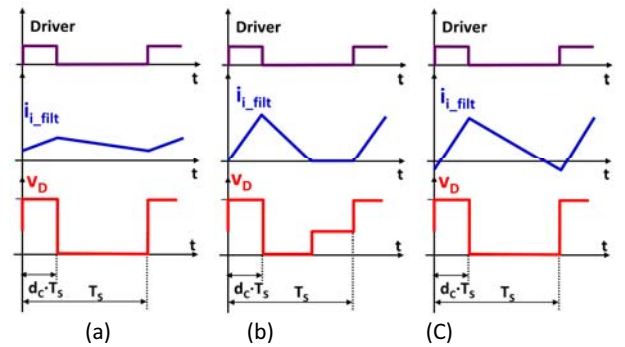


Fig. 16. Current and voltage at the input of the output filter of a classical DC/DC Buck converter (with a second-order LC filter): a) Converter operating in the CCM. b) Converter operating in the DCM. c) Operation in the CCM at light load when the rectifier diode has been replaced with a synchronous rectifier.

the DCM the output voltage depends on the inductor value L , the load R_L and the switching period T_S . Due to this, operation in the DCM is not adequate to use the Buck converter as EA operating in open loop. It should be noted that operation in closed loop to compensate the lack of linearity would decrease the overall system bandwidth. For this reasons, operation in the DCM must be avoided.

The boundary between both modes depends on the value of the dimensionless parameter k and on the boundary value k_{crit} [28]. The operation in CCM is guaranteed if $k > k_{crit}$, whereas the operation in DCM is guaranteed if $k < k_{crit}$. The value of k_{crit} for the Buck converter is [28]:

$$k_{crit} = 1 - d_c \quad (16)$$

Therefore, the operation in the CCM in a classical Buck converter in steady state is guaranteed for any duty cycle if $k > 1$. To illustrate the analysis procedure, the following subsection addresses the study of the conduction mode of a Buck converter with a fourth order filter in steady state conditions.

VI.1 Analysis of the conduction mode in steady state

The first step is to analyse how the voltage across capacitor C_2 is in comparison with the voltage across the load. To do that, the Bode plots corresponding to the transfer functions between the input voltage and the output voltage, v_O/v_g , and the transfer functions between the input voltage and the voltage across C_2 , v_{C2}/v_g , have been drawn in Fig. 17 for the fourth-order types of the filters under study. As this figure shows, the transfer functions of v_{C2}/v_g exhibit significant attenuation above the cut-off frequency, although lower than the corresponding to the transfer functions of v_O/v_g . However, they are sufficient to ensure that the component at the switching frequency, ω_s , across C_2 is relatively small. For example, assume a Buck converter operating with a duty cycle $d_c = 0.5$ from a DC voltage source $v_{DC} = 12$ V; the peak voltage corresponding to the switching-frequency harmonic at the input of the output filter is 7.64 V. If a fourth-order filter with 40 dB attenuation at ω_s is used, then the attenuation at ω_s just across C_2 will be 29.23 dB (Bessel-Thomson filter), 26.66 dB (Butterworth filter) or 23.95 dB (Legendre-Papoulis filter). This means that the filter output voltage will have a DC voltage of 6 V and an AC ripple of approximately 76.4 mV in the three cases, whereas the DC voltage across C_2 will have a DC value of also 6 V, but AC voltage ripples of 264 mV (Bessel-Thomson filter) or 355 mV (Butterworth filter) or 485 mV (Legendre-Papoulis filter). Therefore, the relative ripples across C_2 will be 4.4 %, 5.9 % and 8.1 %, respectively. These low values of relative voltage ripples across C_2 suggest the following approximation to calculate the current through L_1 : the voltage across C_2 can be considered approximately equal to the output voltage, i.e. $v_{C2} \approx v_O$. Thus, the current through L_1 is very similar to that of a conventional Buck, i.e., simple up and down ramps, as those shown in Fig. 16. Furthermore, under this assumption the current ripple in L_3 is negligible and thus L_1 is the only inductor that has to be considered to determine the conduction mode.

Table 7 shows attenuation values provided by the first filter section L_1C_2 at ω_s for the filters under consideration. It can be

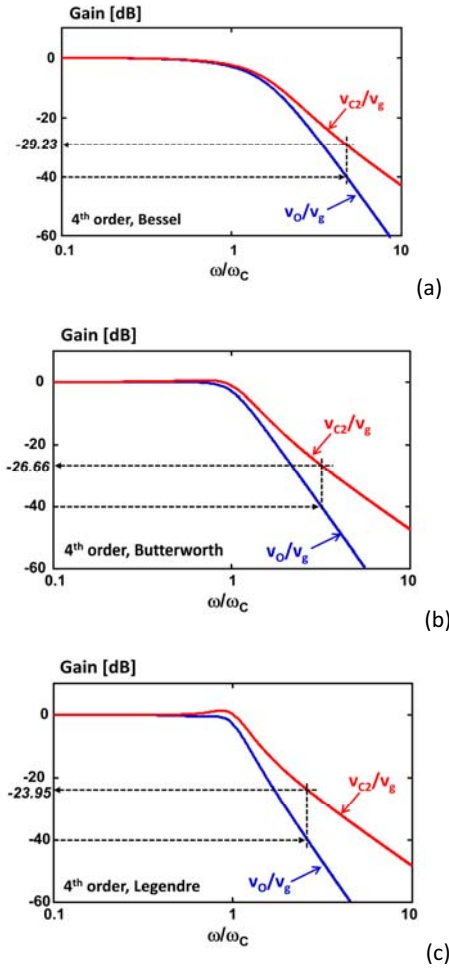


Fig. 17. Transfer functions between the input voltage and output voltage and between the input voltage and the voltage across capacitor C_2 , for the case of a fourth-order Bessel-Thomson filter (a), a Butterworth filter (b) and a Legendre-Papoulis filter (c).

seen that these values are relatively high in all cases and thus the previous conclusion can be extended to all filter families. However, it should be noted that the proposed approximation should not be applied to very-high order filters (especially in the case of Butterworth and Legendre-Papoulis filters), as the attenuation decreases for higher order filters.

Order	Bessel-Thomson		Butterworth		Legendre-Papoulis	
	30 dB @ ω_s	40 dB @ ω_s	30 dB @ ω_s	40 dB @ ω_s	30 dB @ ω_s	40 dB @ ω_s
3 rd	25.8 dB	33.39 dB	24.56 dB	31.95 dB	22.82 dB	30.05 dB
4 th	23.07 dB	29.23 dB	20.78 dB	26.26 dB	18.30 dB	23.95 dB
5 th	21.31 dB	26.57 dB	18.10 dB	23.06 dB	14.50 dB	19.12 dB
6 th	20.17 dB	24.81 dB	16.10 dB	20.43 dB	12.08 dB	16.06 dB

Table 7. Attenuations of the switching-frequency harmonic across C_2 for the filters under study when they have been designed to have an attenuation of 30 dB and 40 dB across the load.

Provided that the aforementioned assumption $v_{C2} \approx v_0$ holds true, the criterion used to determine the conduction mode in a conventional DC/DC Buck converter with a simple LC filter and operating in steady state can also be applied here. Taking into account (11), the dimensionless parameter k given by (15) becomes:

$$k = \frac{l_1}{\pi} \cdot \frac{\omega_S}{\omega_C} . \quad (17)$$

As the operation in the CCM in steady state is guaranteed if $k > k_{\text{crit}}$ and the maximum possible value of k_{crit} is 1 (according to (16)), then the operation in the CCM in steady state will be guaranteed if the ratio ω_S/ω_C satisfies:

$$\frac{\omega_S}{\omega_C} > \frac{\pi}{l_1} . \quad (18)$$

Table 8 shows the values of π/l_1 for the different types and orders of the filters under study. These values also represent a lower limit for the quotient ω_S/ω_C in the plots given in Fig. 10 when the operation in the DCM would occur. In most cases, a practical choice of the ratio ω_S/ω_C to have reasonable attenuation leads to operation in the CCM, as shown in Fig. 18, where Fig. 10 has been re-drawn highlighting the above mentioned lower limits.

VI.2 Analysis of the conduction mode during transients

The study carried out so far has assumed that the Buck converter is operating in steady-state. However, when this converter is used as EA it operates under highly-varying dynamic conditions, continuously changing its operating point as it tracks the envelope waveform to be reproduced. To address this case, the average value (averaged in a switching period) of the current through L_1 , i_{L1_avg} , has been computed. This averaging operation eliminates all the harmonic components corresponding to the switching frequency, its side-bands and above. Current i_{L1_avg} can be easily calculated from the average voltage (also averaged in a switching period, i.e., also excluding the switching frequency, its side-band and its harmonics) of the filter input voltage v_{D_avg} (see Fig. 4) and from the voltage across C_2 , v_{C2} , as follows:

$$i_{L1_avg} = \frac{v_{D_avg} - v_{C2}}{sL_1} . \quad (19)$$

This equation can be re-written taking into account that the v_{D_avg} is equivalent to the input voltage v_g of the filter in Fig. 15b. The final result is:

Order	Bessel-Thomson	Butterworth	Legendre-Papoulis
1 st	3.1416	3.1416	3.1416
2 nd	2.3072	2.2215	2.2215
3 rd	2.1474	2.0944	1.9747
4 rd	2.0929	2.0524	1.9489
5 rd	2.0771	2.0333	1.9189
6 nd	2.0770	2.0230	1.9217

Table 8. Values of the quotient π/l_1 (i.e., the minimum values of the quotient ω_S/ω_C) needed to guarantee the CCM in steady-state when the Buck-derived converter has been implemented with a diode as rectifier.

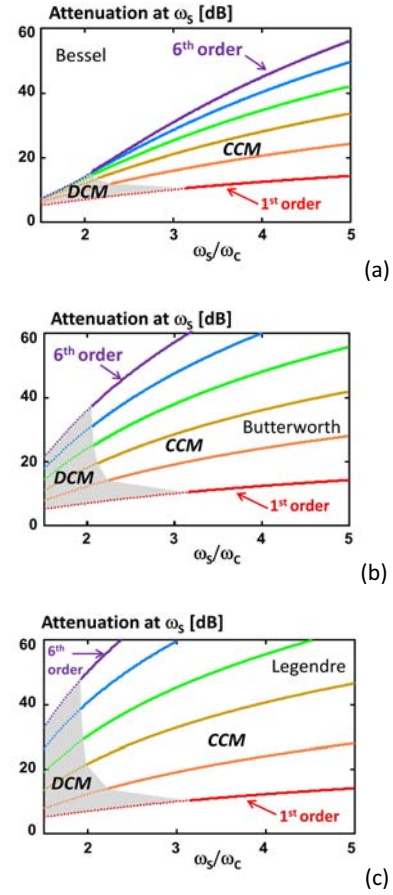


Fig. 18. Attenuation of the angular switching frequency ω_S as a function of the quotient ω_S/ω_C for Bessel-Thomson filters (a), Butterworth filters (b) and Legendre-Papoulis filters (c). In all cases, the areas of operation in both CCM and DCM have been highlighted.

$$i_{L1_avg} = \frac{1 - v_{C2}}{sL_1} \cdot v_g . \quad (20)$$

Equation (20) allows determining the evolution of i_{L1_avg} for a given evolution of v_g , since the transfer function v_{C2}/v_g and the value of L_1 are known. For instance, the average values of the normalized current through L_1 when a voltage step is applied at the filter input (normalized to its final value) are given in Fig. 19. As this figure shows, this current does not suffer noticeable overshoot in the case of the Bessel-Thomson filters. Moreover, the evolution of the current is almost independent of the filter order for orders higher than 2. On the other hand, Butterworth and Legendre-Papoulis filters exhibit a moderate overshoot (lower than 16%) and their response depends on the filter order.

To evaluate the validity of the previous approach to determine the conduction mode during a transient, Fig. 20 shows the current through L_1 , i_{L1} , the average value of i_{L1} during a switching period as given by (20), i_{L1_avg} , and the steady-state value of i_{L1_avg} according to the duty cycle the converter is operating at, $i_{L1_avg_ss}$. It is assumed that the converter has been designed to operate in the CCM in steady state for any duty cycle d_c , which means that not only (16) is

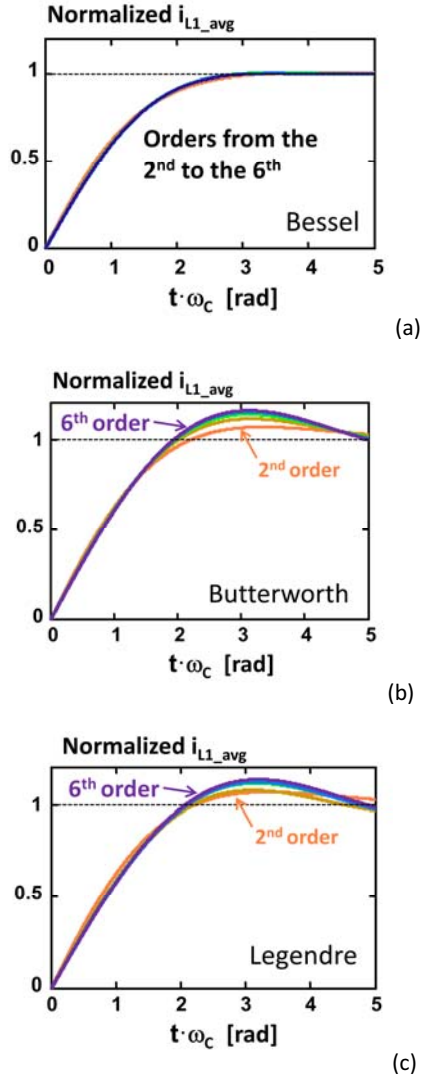


Fig. 19. Response of the normalized average current passing through L_1 when a rising voltage step has been applied at the input of the filter. a) Bessel-Thomson filters. b) Butterworth filters. c) Legendre-Papoulis filters.

satisfied, but also (18). If a rising voltage step takes place at the filter input and the converter was operating in steady-state just before that event, then the converter will continue operating in the CCM after the step because the current through the inductor increases (see Fig. 20a for the particular case of a Bessel-Thomson filter). In the case of a falling voltage step (see Fig. 20b also for the particular case of a Bessel-Thomson filter), the converter will continue working in the CCM only if the value of i_{L1_avg} is higher than $i_{L1_avg_ss}$, since the converter has been designed to operate in CCM in steady state. As Fig. 20b shows, this is only guaranteed if the filter has no overshoot, i.e. only for Bessel-Thomson filters. However, i_{L1_avg} may become smaller than $i_{L1_avg_ss}$ when a falling voltage step takes place at the input of Butterworth or Legendre-Papoulis filters, due to the overshoot that these filters exhibit. This situation is shown in Fig. 20c, where the

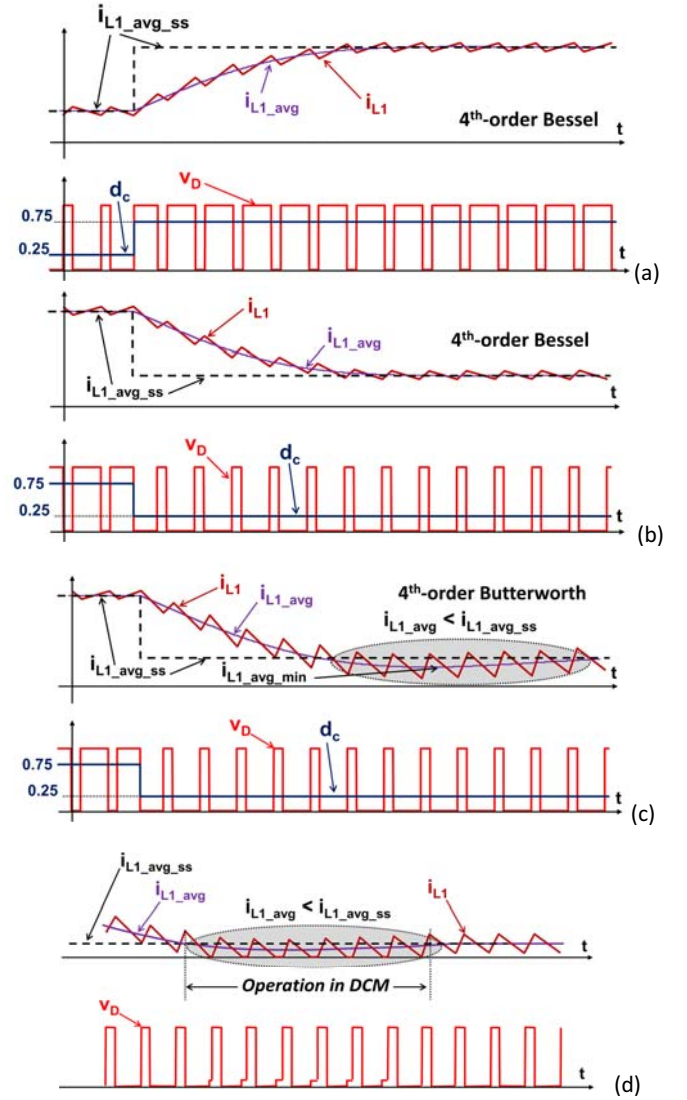


Fig. 20. Current passing through L_1 when a voltage step has been applied at the input of the filter. a) Rising voltage step for a Bessel-Thomson filter. b) Falling voltage step for a Bessel-Thomson filter. c) Falling voltage step for a fourth-order Butterworth filter. d) Operation in DCM during a part of the transient response when $i_{L1_avg} < i_{L1_avg_ss}$.

transient response of a fourth-order Butterworth filter to a falling voltage step is given. As this figure shows, there is a time interval during which i_{L1_avg} is lower than the value of $i_{L1_avg_ss}$. Therefore, the converter is operating in the DCM during several cycles, although the value of L_1 was chosen high enough to guarantee operation in the CCM in steady state.

To derive an expression equivalent to (18) that guarantees CCM operation during transients, it is useful to compute the minimum value of i_{L1_avg} during a falling step when the duty cycle d_c changes from d_{c_up} to d_{c_down} :

$$i_{L1_avg_min} = \frac{v_0}{R_L} \left(1 - \frac{d_{c_up} - d_{c_down}}{d_{c_down}} \xi \right). \quad (21)$$

ξ being the percentage overshoot in the step response of i_{L1_avg} . The maximum value of ξ obtained in Fig. 19b and Fig. 19c is approximately 16%.

It should be noted that the dimensionless parameter k is a measurement of the ratio between the average inductor current in steady-state (which is proportional to $1/R_L$) and the current ripple (which is proportional to T/L_1). During the transient interval of the falling step, the average inductor current is not v_O/R_L but it is changing, its minimum value being given by (21). As a consequence, the minimum value of k during the transient will be:

$$k_{trans_min} = \frac{2L_1}{R_L T_s} \left(1 - \frac{d_{c_up} - d_{c_down}}{d_{c_down}} \xi \right) = k \left(1 - \frac{d_{c_up} - d_{c_down}}{d_{c_down}} \xi \right). \quad (22)$$

Taking into account (16), (22) becomes:

$$k > \frac{(1 - d_{c_down}) d_{c_down}}{d_{c_down} (1 + \xi) - d_{c_up} \xi}. \quad (23)$$

It should be noted that the use of (23) instead of (16) is only necessary when Butterworth or Legendre-Papoulis filters are used, as Bessel filters produce no current overshoot. Moreover, this expression is only valid for values of $i_{L1_avg_min} > 0$, which implies a limit value for the duty cycle:

$$d_{c_lim} = \frac{\xi}{1 + \xi} d_{c_up}. \quad (24)$$

Taking into account (11), (23) finally becomes:

$$\frac{\omega_s}{\omega_c} > \frac{\pi}{l_1} \cdot \frac{(1 - d_{c_down}) d_{c_down}}{d_{c_down} (1 + \xi) - d_{c_up} \xi}. \quad (25)$$

This is the condition to guarantee the operation always in CCM when a falling step from d_{c_up} to d_{c_down} takes place. However, operation always in the CCM during the transient is not possible if $d_{c_down} < d_{c_lim}$.

VII. Design procedure

The design procedure of the output filters described in this paper is illustrated in this section by two design examples.

VII.1. Design example 1

The objective is to design the output filter of a Buck EA operating at 1 MHz. The converter load is 6.4 Ω . The envelope waveform to be reproduced is chosen to be defined by (5), but its frequency should be as high as possible while keeping a 10 % maximum error when reproducing its highest-frequency harmonic. The switching frequency must be attenuated 40 dB at the output of the filter.

Implementation 1.1

As the waveform to be reproduced is band-limited and in order to minimize implementation complexity, a fourth-order Legendre-Papoulis filter will be used.

The design procedure begins by finding the ratio ω_s/ω_c from Fig. 10c (40 dB and fourth-order), which is $\omega_s/\omega_c = 2.59$. Similarly, the value of $\omega_c/\omega_{h_max} = 1.2$ is obtained from Fig. 9c (error lower than 10%). Therefore, the filter cut-off frequency will be 1 MHz/2.59 = 384.6 kHz and the frequency of the highest harmonic of the waveform will be 384.6 kHz/1.2 = 320.5 kHz. By definition of the waveform, this frequency corresponds to the fifth harmonic of the fundamental frequency component, and thus the fundamental,

third and fifth harmonic frequencies are 64.1 kHz, 192.3 kHz and 320.5 kHz, respectively.

The values of the inductors and capacitors of this filter can be computed from the values of Table 6 and from (11) and (12). Table 9 summarizes the results. Finally, operation in CCM in steady-state is guaranteed because $\omega_s/\omega_c = 2.59$ is higher than the ratio $\pi/l_1 = 1.9489$.

To illustrate the impact of the order and the type of the filter over the waveform that the filter can reproduce in the above mentioned conditions, three additional designs are presented, two of them based on Legendre-Papoulis filters (second-order and sixth-order filters) and other based on a fourth-order Butterworth filter.

Implementation 1.2

In the case of a design based on a second-order Legendre-Papoulis filter, the value of the ratio ω_s/ω_c must be 10 to obtain the desired attenuation (40 dB), whereas the value of ω_c/ω_{h_max} must be 1.008 (both values have been mathematically obtained because they are placed out of the range of values of Fig. 10c and Fig. 9c). Therefore, the filter cut-off frequency in this design will be 1 MHz/10 = 100 kHz and the frequency of the highest harmonic of the waveform will be 100 kHz/1.008 = 99.21 kHz. Therefore, the fundamental, third and fifth harmonic frequencies of the waveform that could be reproduced in this case are 19.84 kHz, 59.52 kHz and 99.21 kHz, respectively. Therefore, the frequencies corresponding to the waveform that can be reproduced in the same conditions as in the first implementation is 3.23 times lower, which means worse performance as EA.

Implementation 1.3

A sixth-order Legendre-Papoulis filter is implemented in this case. The value of the ratio ω_s/ω_c obtained from Fig. 10c is 1.685, whereas the value of ω_c/ω_{h_max} obtained from Fig. 9c is 1.351. The filter cut-off frequency will be 1 MHz/1.685 = 593.47 kHz and the frequency of the highest harmonic of the waveform will be 593.47 kHz/1.351 = 439.28 kHz. Therefore, the fundamental, third and fifth harmonic frequencies of the waveform that could be reproduced in this case are 87.86 kHz, 263.57 kHz and 439.28 kHz, respectively. Although this design could seem to be more appropriate than the one based on a fourth order filter, several problems arise.

Thus, this design does not verify the conditions to operate in the CCM in steady-state ($\pi/l_1 = 1.9217$ is higher than $\omega_s/\omega_c = 1.685$). As a consequence, it is not possible for the converter to operate in open loop when a diode is used as rectifier. It should be noted that the operation in closed loop with a high-order filter exhibits huge limitations due to the phase lag of these filters around the cut-off frequency (for example, 352 degrees at ω_c and 142 degrees at $\omega_c/2$).

Moreover, the voltage ripple at the output is likely to be

f_s [MHz]	Att @ f_s	f_c [kHz]	e(320.5kHz)	L_1 [μ H]	C_2 [nF]	L_3 [μ H]	C_4 [nF]
1	40 dB	384.6	<10%	4.27	107.43	3.79	41.38

Table 9. Design example 1, Implementation 1.1.

higher than the expected due to the influence of the lower-side band around the switching frequency (see Fig. 5b). As the ratio ω_s/ω_c is so low in this design, the influence of this side band on the output voltage ripple will probably be significant in comparison with the one corresponding to the switching frequency, thus increasing the total output ripple.

However, a so high-order filter would be useful if the switching-frequency attenuation needed were clearly higher (e.g., 60 dB). In this case, the ratio ω_s/ω_c obtained from Fig. 10c would be 2.371 and, therefore, the converter would operate in the CCM. As the value of ω_c/ω_{h_max} would be 1.351, the harmonic content reproduced by the EA would be 62.44 kHz, 187.31 kHz and 312.19 kHz, which is very similar to the one obtained in Implementation 1.1.

Implementation 1.4

To compare the behaviour of Legendre-Papoulis and Butterworth filters, a fourth-order Butterworth filter has also been designed for this case. The ratios ω_s/ω_c and ω_c/ω_{h_max} are 3.163 (Fig. 10b) and 1.202 (Fig. 9b), respectively. Therefore, the filter cut-off frequency is 316.16 kHz, whereas the harmonic content reproduced by the EA would be 52.60 kHz, 157.81 kHz and 263.02 kHz, which is a slightly worse design than the one obtained in Implementation 1.1.

VII.2. Design example 2

The objective in this case is also to design the output filter of a Buck EA operating at 1 MHz and with a load of 6.4 Ω . As in the previous case, the switching frequency must be attenuated by 40 dB at the output of the filter. The input voltage is 12 V. On the other hand, the filter selected in this case must allow the highest possible slew rate, compatible with the absence of overshoot. Due to this, a Bessel-Thomson filter is selected. To balance performance and implementation simplicity, a fourth order filter is selected once again.

The design procedure begins by obtaining the ratio ω_s/ω_c from Fig. 10a ($\omega_s/\omega_c = 4.723$) and, therefore, the filter cut-off frequency (211.7 kHz). The normalized value of the slew rate just at the middle of a voltage step is given in Table 3 ($nslw_{0.5} = 0.444 \text{ rad}^{-1}$). The maximum slew rate that can be achieved when a voltage step of 10 V takes place is easily obtained from (10), the result being $slw_{0.5} = 0.444 \cdot 2 \cdot \pi \cdot 211.7 \cdot 10^3 \cdot 10 = 5.9 \text{ V}/\mu\text{s}$. The values of the inductors and capacitors of this filter are also computed using (11) and (12), but in this case from the values of I_x and c_x obtained from Table 4. The design parameters are summarized in Table 10. The converter will operate in the CCM in steady-state because the ratio $\omega_s/\omega_c = 4.723$ is higher than the ratio $\pi/I_1 = 2.0929$ (Table 8). Furthermore, as it is a Bessel-Thompson filter, this also guarantees operation in the CCM during transients.

f_s [MHz]	Att @ f_s	f_c [kHz]	$slw_{0.5}$ [V/ μ s]	L_1 [μ H]	C_2 [nF]	L_3 [μ H]	C_1 [nF]
1	40 dB	211.7	5.9	7.22	114.9	2.95	24.83

Table 10. Design example 2.

VIII. Simulation and experimental results

VIII.1. Simulation results

The operation of a Buck EA with different fourth-order output filters have been simulated using PSIM.

The Bessel-Thomson filter has been designed to have a cut-off angular frequency of 1 rad/s. The angular switching frequency has been selected to be attenuated by 40 dB by the filter, which means that it should be 4.723 rad/s. The converter where this filter is placed has been used to reproduce a test waveform like the one defined by (5), but its frequency has been selected in such a way that the angular frequency corresponding to the highest harmonic is 1 rad/s, which means that the first harmonic is 1/5 rad/s, and the third one is 3/5 rad/s. The results obtained are shown in Fig. 21a. This figure shows the current through inductor L_1 and the output voltage V_O compared with the signal to be reproduced v_{env_test} . As explained in Section III, v_{env_test} has been delayed the time

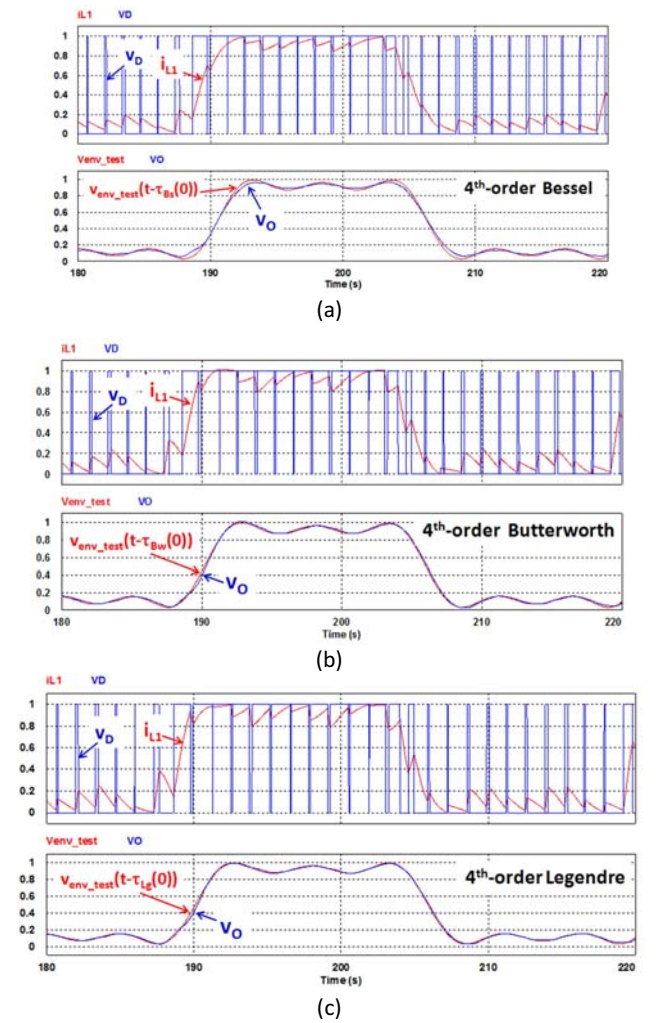


Fig. 21. Simulated results obtained testing a waveform like the one given in (5) in a Buck converter with different types of fourth-order filters, in all cases designed to attenuate the switching frequency by 40 dB: a) Bessel-Thomson filter. b) Butterworth filter. c) Legendre-Papoulis filter.

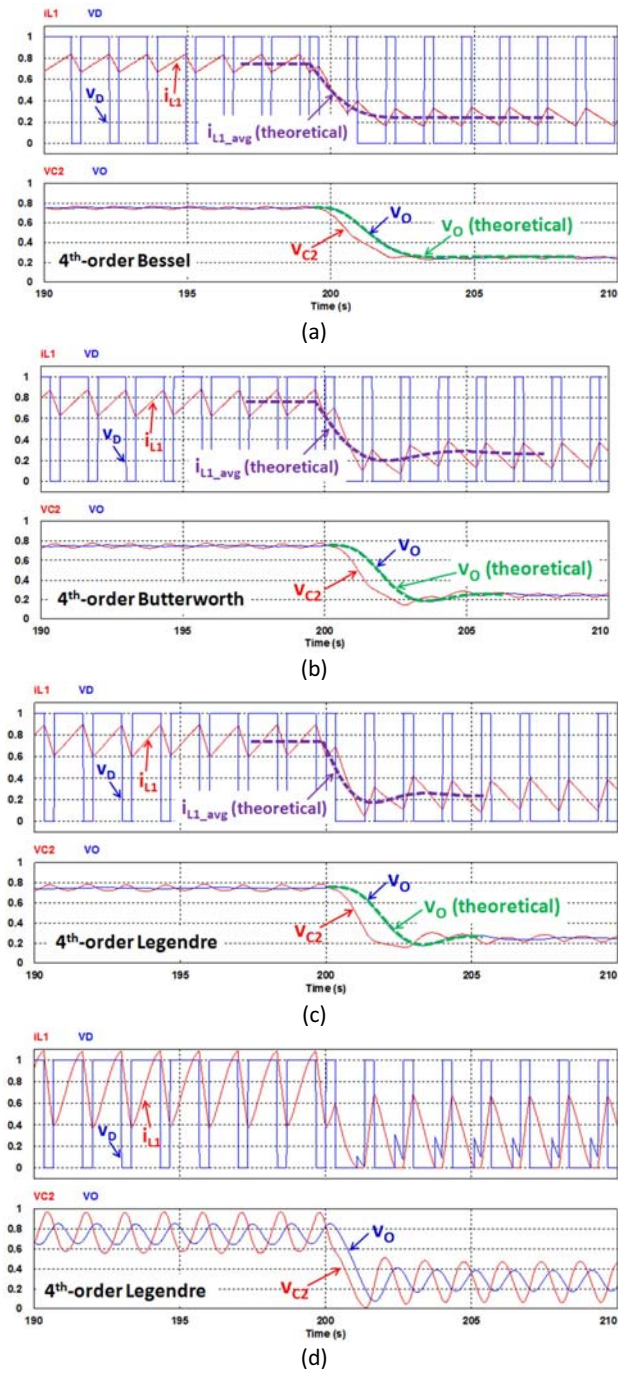


Fig. 22. Simulated results obtained testing a falling voltage step in a Buck converter with a Bessel-Thomson filter (a), a Butterworth filter (b) and a Legendre-Papoulis filter (c), in all cases designed to attenuate the switching frequency by 40 dB. In (d), the value of the reactive elements of the Legendre-Papoulis filter have been divided by 2 in order to force the converter to work in the DCM after the voltage step.

corresponding to the group delay at DC, $\tau_{Bs}(0)$. Both the filter and v_{env_test} correspond to those shown in the theoretical example in Fig. 6a. As it can be observed, analytical and simulation results are in very good agreement.

Figure 21b shows the results obtained replacing the Bessel-Thomson filter with a Butterworth filter. The angular switching frequency is 4.723 rad/s (the same as in the previous case). The cut-off angular frequency of this filter has been selected to also attenuate the switching frequency by 40 dB, which means that it must be 1.494 rad/s (instead of 1 rad/s). The signal v_{env_test} is the same as in the previous case. Once again, analytical results (shown in Fig. 6b) and simulation results are in good agreement. Moreover, the comparison between the results shown in Fig. 21a and Fig. 21b shows that better accuracy reproducing the test waveform is obtained with the Butterworth filter, as concluded by the analysis in Section III.

Similar results (slightly better) have been obtained with a Legendre-Papoulis filter, as Fig. 21c shows. The angular switching frequency (4.723 rad/s) and the test waveform are the same as in the two previous cases, whereas the cut-off angular frequency is 1.821 rad/s to attenuate the switching frequency by 40 dB.

The three filters have also been simulated reproducing a falling voltage step, as shown in Fig. 22. To carry out this step, the converter duty cycle has been suddenly changed from 0.75 to 0.25. The waveforms depicted in Fig. 22a, Fig. 22b and Fig. 23c show the actual current through L_1 compared with its average value predicted using (19). These figures also show the simulated and the analytical waveforms of the output voltage v_O , as well as the voltage across capacitor C_2 , v_{C2} . It should be noted that the evolution of v_{C2} and v_O are very similar in all cases, which confirms the validity of the proposed assumptions under the derivations of the conditions to ensure CCM operation. Also note that the voltage ripple across C_2 is always higher than in the output, as expected from the bode plots given in Fig. 17. Regarding the conduction mode, the waveforms of i_{L1} depicted in Fig. 22a, Fig. 22b and Fig. 22c show that the converter is always operating in the CCM. This fact can be predicted by checking the values of the ratio ω_s/ω_c (4.723 for the Bessel-Thomson filter, 3.16 for the Butterworth filter and 2.59 for Legendre-Papoulis one) against the curves in Fig. 18 and the values given in Table 8. Moreover, the values of ω_s/ω_c are also higher than $1.041\pi/l_1$ (2.137 for the Butterworth and 2.029 for the Legendre-Papoulis, respectively), which guarantees operation in CCM both in steady-state and in transient conditions.

Finally, the values of all the reactive elements in the Legendre-Papoulis filter have been divided by 2 in order to force the converter to partially operate in the DCM. The results obtained are given in Fig. 22d, where it can be observed that the converter operates in the CCM just before the falling voltage step (duty cycle $d_c = 0.75$ in steady-state), but it enters into the DCM after the step ($d_c = 0.25$ in steady-state). Now both the ratio ω_s/ω_c and the value of l_1 become divided by 2, which means that k is divided by 4, according to (17). Therefore, $k = 2.59 \cdot 1.612/(\pi \cdot 4) = 0.332$, which is higher than the value of k_{crit} corresponding to $d_c = 0.75$ ($k_{crit} = 1 - 0.75 = 0.25$), but lower than the value of k_{crit} corresponding to $d_c = 0.25$ ($k_{crit} = 1 - 0.25 = 0.75$). Therefore, in steady state it is expected that the converter will operate in the CCM when $d_c =$

0.75 and in the DCM when $d_c = 0.25$. Simulation results shown in Fig. 22d confirm these calculations. Moreover, it should be noted that the design of the output filter in these conditions causes significant output voltage ripple, as well as voltage ripple across C_2 . Thus, this design would have a very poor performance and should be avoided.

VIII.2. Experimental results

Two Buck converters have been built to test their operation as EA. Both converters have the same switching frequency (1 MHz), load (6.4 Ω) and input voltage (8 V). The power devices and all the auxiliary circuitry are also the same in both converters. Thus, the transistor used as power switch is an IPD135N03LG (Infineon), whereas the power diode is a MBRA130 (Semtech Electronics). The floating driving system for the power switch has been designed using a very fast digital isolation integrated circuit IL610 (NVE) and a high frequency driver integrated circuit EL7156 (Intersil). The inductors have been built using iron powder toroidal cores T72-8/90 (Micrometals). The capacitance needed for the filter capacitors have been obtained connecting ceramic and MKT film capacitors (Siemens) in parallel. The PWM control signal is digitally generated using a Virtex 4 FPGA.

The only difference between both converters is the output filter. Thus, one of them has a Legendre-Papoulis filter with the main characteristics of the one corresponding to “**Design example 1, Implementation 1.1**” in Section VII, whose reactive components are given in Table 9. On the other hand, the other one has a Bessel filter with the main characteristics of the “**Design example 2**”. Its reactive components are given in Table 10.

Figures 23 and 24 shows the results obtained from these prototypes. The voltage ripples across C_2 and across the load when the converter is operating with a fixed value of the duty cycle ($d_c = 0.5$) is shown in Fig. 23a (Legendre-Papoulis) and Fig. 24a (Bessel). As the input voltage is 8 V and the duty cycle is 0.5, the AC component at the input of the filter is a square waveform of 4 V, whose first harmonic has a peak value of $4 \cdot 4/\pi = 5.1$ V. Therefore, the voltage ripple at the output should be 51 mV in both designs, because both filters have been designed to attenuate 40 dB. As Fig. 23a and Fig. 24a show, the ripple obtained is very close to this theoretical value.

Figure 23b shows the main waveforms obtained when the test signal v_{env_test} of “**Design example 1, Implementation 1.1**” is reproduced by the prototype with Legendre-Papoulis filter. As it can be seen, the current passing through inductor L_1 is made up of positive and negative ramps, as in the case of a DC/DC converter with a standard second-order filter. As predicted in the theoretical analysis, the converter is working in the CCM, although it is close to DCM operation when reproducing the lower level of the test waveform. The output voltage v_o does not have appreciable voltage ripple, which means that the selected attenuation (40 dB) is high enough for practical applications. The results obtained are in good agreement with those shown in Fig. 21c, the main difference being that the reference signal v_{env_test} has not been delayed as in Fig. 21. Also, the time scale is different, due to the different

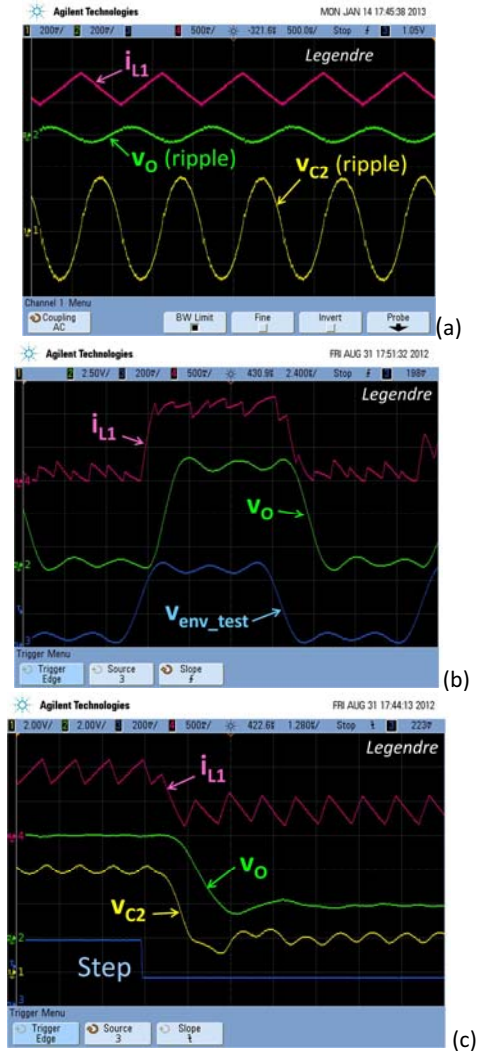


Fig. 23. Experimental results obtained in a Buck EA with a fourth-order Legendre-Papoulis filter: a) Waveforms of i_{L1} (0.5 A/div), ripple of v_o (0.2 V/div) and ripple of v_{C2} (0.2 V/div). b) Testing a waveform like the one given in (5); the time scale is 2.4 μ s/div. c) Testing a falling voltage step from 6 V to 2 V; the time scale is 1.28 μ s/div.

frequencies used in the simulation and experimental results. Slight asymmetries are observed in the experimental waveform, which are mainly due to the non-ideal behaviour of the digital control system.

The test signal v_{env_test} of “**Design example 1, Implementation 1.1**” (Legendre-Papoulis filter) has been reproduced by the prototype with Bessel filter, whose cut-off frequency is 211.7 kHz. The ratio ω_c/ω_{h_max} is in this case $211.7/320.5 = 0.66$, which leads to a quite high value of the quadratic error defined in (6) (in fact, its value is 34%). This is reflected in Fig. 24b. Comparing this figure (Bessel filter) and Fig. 23b (Legendre-Papoulis filter), it can be observed that better accuracy reproducing the test waveform is obtained with the Legendre-Papoulis filter, as concluded by the analysis in Section III.

Both converters have also been tested under a negative voltage step (from $d_c = 0.75$ to $d_c = 0.25$), as shown in Fig. 23c

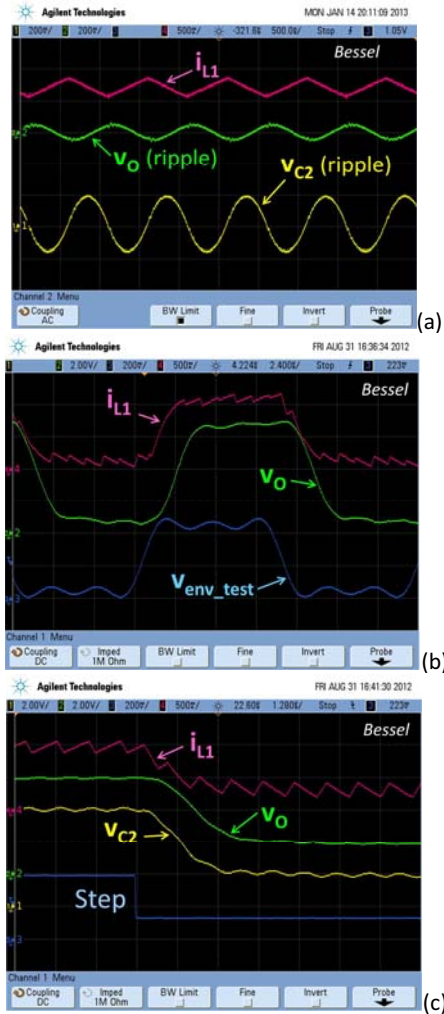


Fig. 24. Experimental results obtained in a Buck EA with a fourth-order Bessel filter: a) Waveforms of i_{L1} (0.5 A/div), ripple of v_O (0.2 V/div) and ripple of v_{C2} (0.2 V/div). b) Testing a waveform like the one given in (5); the time scale is $2.4 \mu\text{s}/\text{div}$. c) Testing a falling voltage step from 6 V to 2 V; the time scale is $1.28 \mu\text{s}/\text{div}$.

and Fig. 24c. The results obtained are in very good concordance with the ones given in Fig. 22c (Legendre-Papoulis filter) and Fig. 22a (Bessel filter), but obviously at the corresponding time scale. The operation in CCM in all conditions clearly appears in these figures. No appreciable ripple is observed on the output voltage v_O (as predicted in Fig. 22c and Fig. 22a), but there is appreciable ripple on the voltage across capacitor C_2 in both cases, as it is also predicted by the simulations. This voltage ripple is properly attenuated by the second part of the filter (inductor L_3 and capacitor C_4). Figure 24c shows that the response corresponding to the Bessel filter does not exhibit any overshoot (as predicted), whereas some overshoot appears in the case of the converter with Legendre-Papoulis filter (see Fig. 23c).

Finally, as the falling step goes from 6 V to 2V, the theoretical slew rate of the output voltage just at the middle of the step should be $slw_{0.5} = 0.444 \cdot 2 \cdot \pi \cdot 211.7 \cdot 10^3 \cdot (6-2) = 2.36$

V/ μs in the case of the Bessel filter, whereas the slew rate measured in the prototype has been $2.08 \text{ V}/\mu\text{s}$. On the other hand, the theoretical slew rate in the case of the converter with Legendre-Papoulis filter should be $slw_{0.5} = 0.352 \cdot 2 \cdot \pi \cdot 384.6 \cdot 10^3 \cdot (6-2) = 3.4 \text{ V}/\mu\text{s}$; the slew rate measured in the prototype has been $3.47 \text{ V}/\mu\text{s}$ in this case.

IX. Conclusions

Bessel-Thomson, Butterworth and Legendre-Papoulis low-pass filters are suitable filters to be used as output filters of Buck DC/DC converters. The proper design of these filters shows that Butterworth and Legendre-Papoulis filters have superior performance compared to Bessel-Thomson filters when reproducing band-limited envelopes. However, they exhibit overshoot when very fast transients (like voltage steps) appear in the envelope signal to be reproduced. From this point of view, Bessel-Thomson filters have better behaviour due their absence of overshoot when a voltage step must be reproduced, although the output voltage variation is slower.

The values of the reactive components in these filters must be calculated from the proper tables, different to the usual ones. This is because the usual tables are for applications where the input voltage source has a specific value of output impedance and the design of the filter is based on obtaining maximum power transfer from this source to the load.

The conduction mode of a Buck converter with a high-order filter has also been addressed in this paper. The conduction mode is important when the converter has been designed with no output-voltage feedback loop (in order to achieve as maximum bandwidth as possible) and with a diode instead of a synchronous rectifier (in order to operate at as high switching frequency as possible). In these conditions, linear dependence between the converter duty cycle and the output voltage only exists if the converter is operating in the CCM. Fortunately, the criterion to guarantee the operation in CCM in the case of standard Buck converters (with a second-order filter) operating in steady-state can be used in the case of high-order filters when they have been designed for reasonable switching-frequency attenuations (e.g., higher than 30 dB for filter orders up to the fourth one). Moreover, the operation in the CCM in transient response can be guaranteed many times if the value of the dimensionless conduction parameter k is properly increased over its critical value k_{crit} .

Finally, the theoretical behaviour of a Buck converter with high-order filters operating in several different situations has been deeply verified by simulating the converter operation with PSIM, showing and excellent concordance with the theoretical assumptions. Moreover, two experimental prototypes using Legendre-Papoulis and Bessel filters have been built and tested, also with good concordance with the theoretical assumptions.

Acknowledgments

This work was supported by the Spanish Ministry of Education and Science under Consolider Project RUE CSD2009-00046, Project DPI2010-21110-C02-0, and European Regional Development Fund (ERDF) grants.

References

- [1] G. Hanington, P. F. Chen, P. M. Asbeck and L. E. Larson, "High-efficiency power amplifier using dynamic power-supply voltage for CDMA applications", **IEEE Transactions on Microwave Theory and Techniques**, vol. 47, no. 8, August 1999, pp. 1471-1476.
- [2] D. Anderson and W. H. Cantrell, "High-efficiency high-level modulator for use in dynamic envelope tracking CDMA RF power amplifiers," **IEEE MTT-S International Microwave Symposium 2001**, vol. 3, pp. 1509-1512.
- [3] B. Sahu and G. Rincón-Mora, "System-level requirements of DC-DC converters for dynamic power supplies of power amplifiers", **IEEE Asia-Pacific Conference 2002**, pp.149-152.
- [4] B. Sahu and G. Rincón-Mora, "A high-efficiency linear RF power amplifier with a power-tracking dynamically adaptive Buck-Boost supply", **IEEE Transactions on Microwave Theory and Techniques**, vol. 52, no. 1, January 2004, pp. 112-120.
- [5] A. Soto, J. A. Oliver, J. A. Cobos, J. Cezón, and F. Arévalo, "Power supply for a radio transmitter with modulated supply voltage," **IEEE Applied Power Electronics Conference 2004**, vol. 1, pp. 392-398.
- [6] N. Wang, V. Yousefzadeh, D. Maksimovic, S. Pajic and Z. Popovic, "60% efficient 10-GHz power amplifier with dynamic drain bias control" **IEEE Transactions on Microwave Theory and Techniques**, vol. 52, no. 3, March 2004, pp. 1077-1081.
- [7] F. Wang, A. H. Yang, D. Kimball, L. Larson, and P. Asbeck, "Design of wide-bandwidth envelope-tracking power amplifiers for OFDM applications," **IEEE Transactions on Microwave Theory and Techniques**, vol. 53, no. 4, April 2005, pp. 1244-1255.
- [8] M. C. W. Høyerby and M. A. E. Andersen, "High-bandwidth, high-efficiency envelope tracking power supply for 40W RF power amplifier using paralleled bandpass current sources" **IEEE Power Electronics Specialists Conference 2005**, pp. 2804-2809.
- [9] V. Yousefzadeh, E. Alarcón, and D. Maksimovic, "Three-level buck converter for envelope tracking applications," **IEEE Transactions on Power Electronics**, vol. 21, no. 2, Mar. 2006, pp. 549-552.
- [10] D. F. Kimball, J. Jeong, C. Hsia, P. Draxler, S. Lanfranco, W. Nagy, K. Linthicum, L. E. Larson and P. M. Asbeck, "High-efficiency envelope-tracking W-CDMA base-station amplifier using GaN HFETs" **IEEE Transactions on Microwave Theory and Techniques**, vol. 54, no. 11, November 2006, pp. 3848-3856.
- [11] M. C. W. Høyerby and M. A. E. Andersen, "Ultrafast tracking power supply with fourth-order output filter and fixed-frequency hysteretic control," **IEEE Transactions on Power Electronics**, vol. 23, no. 5, September 2008, pp. 2387-2398.
- [12] M. Rodríguez, P. Fernández-Miaja, A. Rodríguez and J. Sebastián, "A multiple-input digitally controlled Buck converter for envelope tracking applications in radiofrequency power amplifiers" **IEEE Transactions on Power Electronics**, vol. 25, no. 2, February 2010, pp. 369-381.
- [13] M. Rodríguez, P. Fernández-Miaja, J. Sebastián, and Dragan Maksimovic, "Mismatch-error shaping-based digital multiphase modulator" **IEEE Transactions on Power Electronics**, vol. 27, no. 4, April 2012, pp. 2055-2066.
- [14] P. Fernández-Miaja, M. Rodríguez, A. Rodríguez and J. Sebastián. "A linear assisted DC/DC converter for Envelope Tracking and Envelope Elimination and Restoration applications", **IEEE Transactions on Power Electronics**, vol. 27, no.7, July 2012, pp. 3302-3309.
- [15] H. Huang, J. Bao and L. Zhang, "A MASH-controlled multilevel power converter for high-efficiency RF transmitters", **IEEE Transactions on Power Electronics**, vol. 26, no. 4, April 2012, pp. 1205-1214.
- [16] X. Xiong, X. Ruan, H. Xi, and J. Ge, "Feed-forwarding the output voltage to improve efficiency for Envelope-Tracking power supply based on a switch-linear hybrid scheme". **IEEE Transactions on Power Electronics**, vol. 26, no. 8, August 2011, pp. 2106-2111.
- [17] G. Gong, H. Ertl and J. W. Kolar "Novel tracking power supply for linear power amplifier", **IEEE Transactions on Industrial Electronics**, vol. 55, no. 2, February 2008, pp. 684-698.
- [18] G. Gong, D. Hassler and J. W. Kolar "A comparative study of multicell amplifiers for AC-power-source applications" **IEEE Transactions on Power Electronics**, vol. 26, no. 1, January 2011, pp. 149-164.
- [19] L. R. Kahn, "Single-sideband transmission by envelope elimination and restoration" **Proceeding of the IRE**, July 1952, pp. 803-806.
- [20] F. H. Raab, B. E. Sigmon, R. G. Myers, and R. M. Jackson, "L-Band transmitter using Kahn EER technique", **IEEE Transactions on Microwave Theory and Techniques**, vol. 46, no. 12, December 1998, pp. 2220-2225.
- [21] D. Milosevic, J. van der Tang and A. van Roermund, "Intermodulation products in the EER technique applied to Class-E amplifiers" **IEEE International Symposium on Circuits and Systems 2004**, pp. 637-640.
- [22] N. Wang, X. Peng, V. Yousefzadeh, D. Maksimovic, S. Pajic and Z. Popovic, "Linearity of X-band Class-E power amplifiers in EER operation", **IEEE Transactions on Microwave Theory and Techniques**, vol. 53, no. 3, March 2005, pp. 1096-1102.
- [23] V. Yousefzadeh, N. Wang, Z. Popovic, and D. Maksimovic, "A digitally controlled DC/DC converter for an RF power amplifier" **IEEE Transactions on Power Electronics**, vol. 21, no. 1, January 2006, pp. 64-172.
- [24] F. Wang, D. F. Kimball, J. D. Popp, A. H. Yang, D. Y. Lie, P. M. Asbeck and L. E. Larson, "An improved power-added efficiency 19-dBm hybrid envelope elimination and restoration power amplifier for 802.11g WLAN applications", **IEEE Transactions on Microwave Theory and Techniques**, vol. 54, no. 12, December 2006, pp. 4086-4099.
- [25] M. Vasic, O. García, J. A. Oliver, P. Alou, D. Díaz, R. Prieto and J. A. Cobos, "Envelope amplifier based on switching capacitors for high-efficiency RF amplifiers", **IEEE Transactions on Power Electronics**, vol. 27, no.3, March 2012, pp. 1359- 1368.
- [26] M. Vasic, O. García, J. A. Oliver, P. Alou, D. Díaz, J. A. Cobos, A. Gimeno, J. M. Pardo, C. Benavente and F. J. Ortega, "Efficient and linear power amplifier based on Envelope Elimination and Restoration", **IEEE Transactions on Power Electronics**, vol. 27, no. 1, January 2012, pp. 5-9.
- [27] M. Bathily, B. Allard, F. Hasbani, V. Pinon, and J. Verdier, "Design flow for high switching frequency and large-bandwidth analog DC/DC step-down converters for a polar transmitter", **IEEE Transactions on Power Electronics**, vol. 27, no. 2, February 2012, pp. 838-847.
- [28] S. Cuk and R. D. Middlebrook, "A general unified approach to modelling switching dc-to-dc converters in discontinuous conduction mode" **IEEE Power Electronics Specialists Conference 1977**, p. 36-57.
- [29] R. Schaumann, M. S. Ghauri and K. R. Laker, "Design of analog filters", **Prentice-Hall Inc.** 1990. ISBN 0-13-200288-4.
- [30] W. J. Kerwin, "Electrical Engineering Handbook. Chapter 4: Passive Signal Processing". **CRC Press Inc.** 1993. ISBN 0-8493-0185-8.
- [31] E. C. Jones, H. W. Hale, A. B. Williams and F. J. Taylor, "Electronics Engineers' Handbook. Chapter 16: Filters and Attenuators", **McGraw-Hill Companies Inc.** 1996. IEEE press. ISBN 0-07-021077-2.

[32] D. G. Holmes and T. A. Lipo, "Pulse Width Modulation for Power Converters: Principles and Practice", **John Wiley & Sons**, 2003.

[33] L. Marco, A. Poveda, E. Alarcón and D. Maksimovic, "Bandwidth limits in PWM switching amplifiers", **IEEE International Symposium on Circuits and Systems 2006**, pp. 5323-5326.

[34] L. Marco, E. Alarcón and D. Maksimovic, "Effects of switching power converter nonidealities in Envelope Elimination and Restoration technique", **IEEE International Symposium on Circuits and Systems 2006**, pp. 3137-3140.

[35] F. F. Kuo, Network analysis and synthesis". **John Wiley and Sons, Inc.**

[36] G. C. Temes and J. W. LaPatra, "Introduction to circuit synthesis and design", **McGraw-Hill, Inc.** 1977. ISBN 0-07-063489-0.



Javier Sebastián (M'87-SM'11) was born in Madrid, Spain, in 1958. He received the M.Sc. degree from the Polytechnic University of Madrid, and the Ph.D. degree from the University of Oviedo, Spain, in 1981 and 1985, respectively. He was an Assistant Professor and an Associate Professor at both the Polytechnic University of Madrid and at the University of Oviedo, in

Spain. Since 1992, he has been with the University of Oviedo, where he is currently a Professor. His research interests are switching-mode power supplies, modelling of dc-to-dc converters, low output voltage dc-to-dc converters and high power factor rectifiers.



Pablo F. Miaja (S'07 M'13) was born in Oviedo, Spain, in 1984. He received the M.S. degree in telecommunication engineering from the University of Oviedo in 2007 and in 2012 the Ph.D. degree from the same

university. Since December 2007 he works as a researcher at the Electronic Power Supply Systems Group of the University of Oviedo. His research interests include dc/dc conversion, digital control of switched converters and power-supply systems for RF amplifiers.



Alberto Rodríguez (S'07) was born in Oviedo, Spain, in 1981. He received the M.S. degree in telecommunication engineering in 2006 from the University of Oviedo, Gijón, Spain, where he is currently working towards the Ph.D. degree. In 2006, he has been a Telecommunications Engineer with the Government of the Principality of Asturias and an Assistant Professor with the Department of Electrical Engineering,

University of Oviedo. Since 2007 he has been working in University of Oviedo at full time. His research interests are focused on multiple port power supply systems, bidirectional DC-DC power converters and wide band gap semiconductors.



Miguel Rodríguez (S'06, M'11) was born in Gijón, Spain, in 1982. He received the M.S. degree and the Ph.D. degree in telecommunication engineering from the University of Oviedo in 2006 and 2011, respectively. Since 2011 he works as a postdoctoral Research Associate at the Colorado Power Electronics Center, University of Colorado at Boulder. His research interests include dc/dc conversion,

digital control of switched converters and power-supply systems for RF amplifiers.